

# An Introduction to the BFS Method and Its Use to Model Binary NiAl Alloys

Guillermo Bozzolo  
Ohio Aerospace Institute, Cleveland, Ohio

Ronald D. Noebe  
Lewis Research Center, Cleveland, Ohio

J. Ferrante  
Cleveland State University, Cleveland, Ohio

C. Amador  
Universidad Nacional Autónoma de México, Mexico D.F., Mexico

## The NASA STI Program Office . . . in Profile

Since its founding, NASA has been dedicated to the advancement of aeronautics and space science. The NASA Scientific and Technical Information (STI) Program Office plays a key part in helping NASA maintain this important role.

The NASA STI Program Office is operated by Langley Research Center, the Lead Center for NASA's scientific and technical information. The NASA STI Program Office provides access to the NASA STI Database, the largest collection of aeronautical and space science STI in the world. The Program Office is also NASA's institutional mechanism for disseminating the results of its research and development activities. These results are published by NASA in the NASA STI Report Series, which includes the following report types:

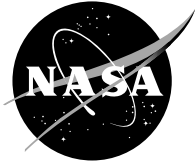
- **TECHNICAL PUBLICATION.** Reports of completed research or a major significant phase of research that present the results of NASA programs and include extensive data or theoretical analysis. Includes compilations of significant scientific and technical data and information deemed to be of continuing reference value. NASA's counterpart of peer-reviewed formal professional papers but has less stringent limitations on manuscript length and extent of graphic presentations.
- **TECHNICAL MEMORANDUM.** Scientific and technical findings that are preliminary or of specialized interest, e.g., quick release reports, working papers, and bibliographies that contain minimal annotation. Does not contain extensive analysis.
- **CONTRACTOR REPORT.** Scientific and technical findings by NASA-sponsored contractors and grantees.

- **CONFERENCE PUBLICATION.** Collected papers from scientific and technical conferences, symposia, seminars, or other meetings sponsored or cosponsored by NASA.
- **SPECIAL PUBLICATION.** Scientific, technical, or historical information from NASA programs, projects, and missions, often concerned with subjects having substantial public interest.
- **TECHNICAL TRANSLATION.** English-language translations of foreign scientific and technical material pertinent to NASA's mission.

Specialized services that complement the STI Program Office's diverse offerings include creating custom thesauri, building customized data bases, organizing and publishing research results . . . even providing videos.

For more information about the NASA STI Program Office, see the following:

- Access the NASA STI Program Home Page at **<http://www.sti.nasa.gov>**
- E-mail your question via the Internet to **[help@sti.nasa.gov](mailto:help@sti.nasa.gov)**
- Fax your question to the NASA Access Help Desk at (301) 621-0134
- Telephone the NASA Access Help Desk at (301) 621-0390
- Write to:  
NASA Access Help Desk  
NASA Center for Aerospace Information  
7121 Standard Drive  
Hanover, MD 21076



# An Introduction to the BFS Method and Its Use to Model Binary NiAl Alloys

Guillermo Bozzolo  
Ohio Aerospace Institute, Cleveland, Ohio

Ronald D. Noebe  
Lewis Research Center, Cleveland, Ohio

J. Ferrante  
Cleveland State University, Cleveland, Ohio

C. Amador  
Universidad Nacional Autónoma de México, Mexico D.F., Mexico

National Aeronautics and  
Space Administration

Lewis Research Center

## **Acknowledgments**

Fruitful discussions with Dr. N. Bozzolo are gratefully acknowledged. C. A. acknowledges partial support from Facultad de Quimica. Computational services by Direccion General de Servicios de Computo Academico are gratefully acknowledged. We would like to thank F. Honey and P. Abel for their helpful comments and suggestions in preparing this manuscript.

This work was partially funded by the HITEMP and PPM programs of NASA Lewis Research Center.

### **Available from**

NASA Center for Aerospace Information  
7121 Standard Drive  
Hanover, MD 21076  
Price Code: A04

National Technical Information Service  
5285 Port Royal Road  
Springfield, VA 22100  
Price Code: A04

# **AN INTRODUCTION TO THE BFS METHOD AND ITS USE TO MODEL BINARY NiAl ALLOYS**

Guillermo Bozzolo<sup>(a)</sup>, Ronald D. Noebe<sup>(b)</sup>, J. Ferrante<sup>(c)</sup> and C. Amador<sup>(d)</sup>

<sup>a</sup> Ohio Aerospace Institute, 22800 Cedar Point Rd., Cleveland, OH 44142, U.S.A.

<sup>b</sup> National Aeronautics and Space Administration, Lewis Research Center,  
Cleveland, OH 44135, U.S.A.

<sup>c</sup> Department of Physics, Cleveland State University, Cleveland, OH 44115, U.S.A.

<sup>d</sup> Departamento de Fisica y Quimica Teorica, Facultad de Quimica, Universidad  
Nacional Autonoma de Mexico, Mexico D. F. , Mexico

## **SUMMARY**

We introduce the Bozzolo-Ferrante-Smith (BFS) method for alloys as a computationally efficient tool for aiding in the process of alloy design. An intuitive description of the BFS method is provided, followed by a formal discussion of its implementation. The method is applied to the study of the defect structure of NiAl binary alloys. The groundwork is laid for a detailed progression to higher order NiAl-based alloys linking theoretical calculations and computer simulations based on the BFS method and experimental work validating each step of the alloy design process.

**Keywords:** Alloys, Intermetallics, BFS Method, Defect Structure, Semiempirical Methods

## INTRODUCTION

A number of industries including the electronics, computer, aeronautics, aerospace, and other transportation related enterprises have long relied on the application of new high-performance materials for their competitive advantages. Yet, in aeronautics and aerospace applications in particular, the potential loss in lives and liability that could result from any material failure dictates that these systems must be very well characterized and understood. Therefore, not only do these new materials have to push the envelope in terms of performance, at the same time they need a high degree of maturity. This makes the introduction of new materials in these industries time consuming and costly due to the need for painstaking development, testing, and characterization. At the same time, without the large defense-related expenditures that were possible during the cold war era, it is necessary to find new ways for industry to operate that will provide significant reductions in expense and cycle time in the development, maturation, and certification processes for new materials. To achieve these goals, the experimental approach to materials research and design will have to be augmented with computational processes. The goal is to develop computational capabilities for alloy design with crystalline materials to the same or greater degree than exists today in the polymer and pharmaceutical industries.

In a series of articles we will describe the integration of a new computational materials model, known as the BFS method [1], into an actual materials design program. The intent of this integrated experimental and computational program is to develop revolutionary new alloys based on the ordered intermetallic compound NiAl as a replacement for Ni-based superalloys in aero-turbine applications. NiAl offers a number of advantages over Ni-based superalloys, including a higher melting temperature, better environmental resistance, significantly higher thermal conduc-

tivity, a better response to thermal barrier coatings, and a reduction in density by as much as a third without significantly impacting creep strength [2]. However, the development of an alloy composition with the correct balance of high temperature strength and low temperature fracture resistance has continued to elude investigators [3], leading to continued alloy design-structure-property investigations and the eventual integration of computational processes (BFS method) in the search for an acceptable alloy.

Through the eventual partnership between experimental and theoretical procedures, we were able to determine the naturally evolving role of computational methods in an alloy design program. This role is schematically illustrated in Figure 1. At first, the design approach reported in this work was guided by past experimental work of an empirical nature. For most alloy design programs this is essentially one continuous loop (Figure 1.a). But an integrated alloy design program that augments experimental results with theoretical modeling would follow the path described in Figure 1.b. We started by modeling what was known about the NiAl system. This allowed us to establish confidence in the model, make changes and optimize the model, and to help understand and interpret the results. The model also provided the energetic explanations for many of the experimental observations, thus giving us greater insight into the alloy system. As confidence in the model grew, we started filling the gaps in our experimental database with computational results. Finally, as alloy compositions became more complicated and burdensome to evaluate, we used the computational model to direct the experimental work, and only experimentally verified those few compositions that looked promising or that we needed in order to refine the model. The advantage of this integrated approach is that it funnels most of the alloys through a virtual production and screening process significantly reducing the number of alloys actually produced and characterized. This saves significant time and expense since the experimental process is

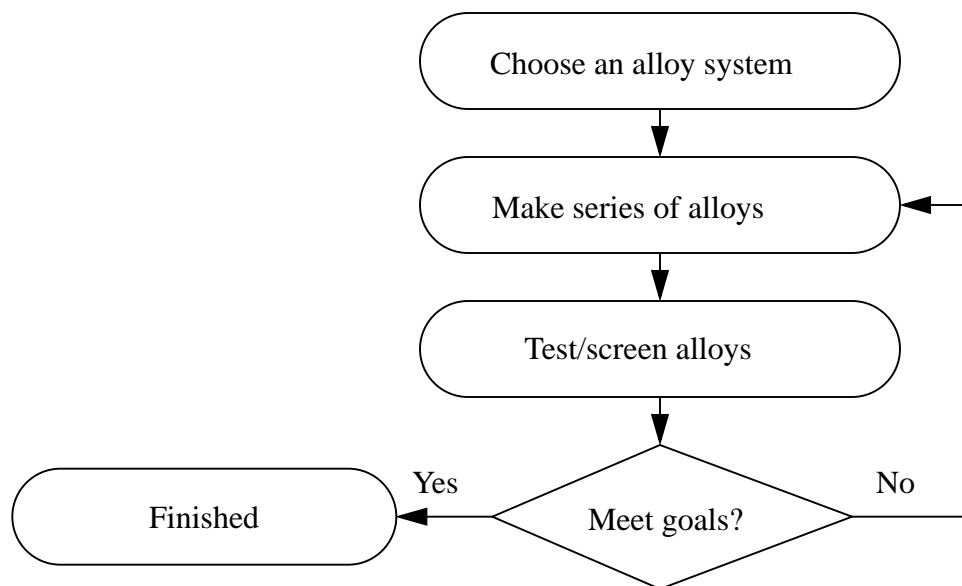


Figure 1.a Conventional Alloy Design Program

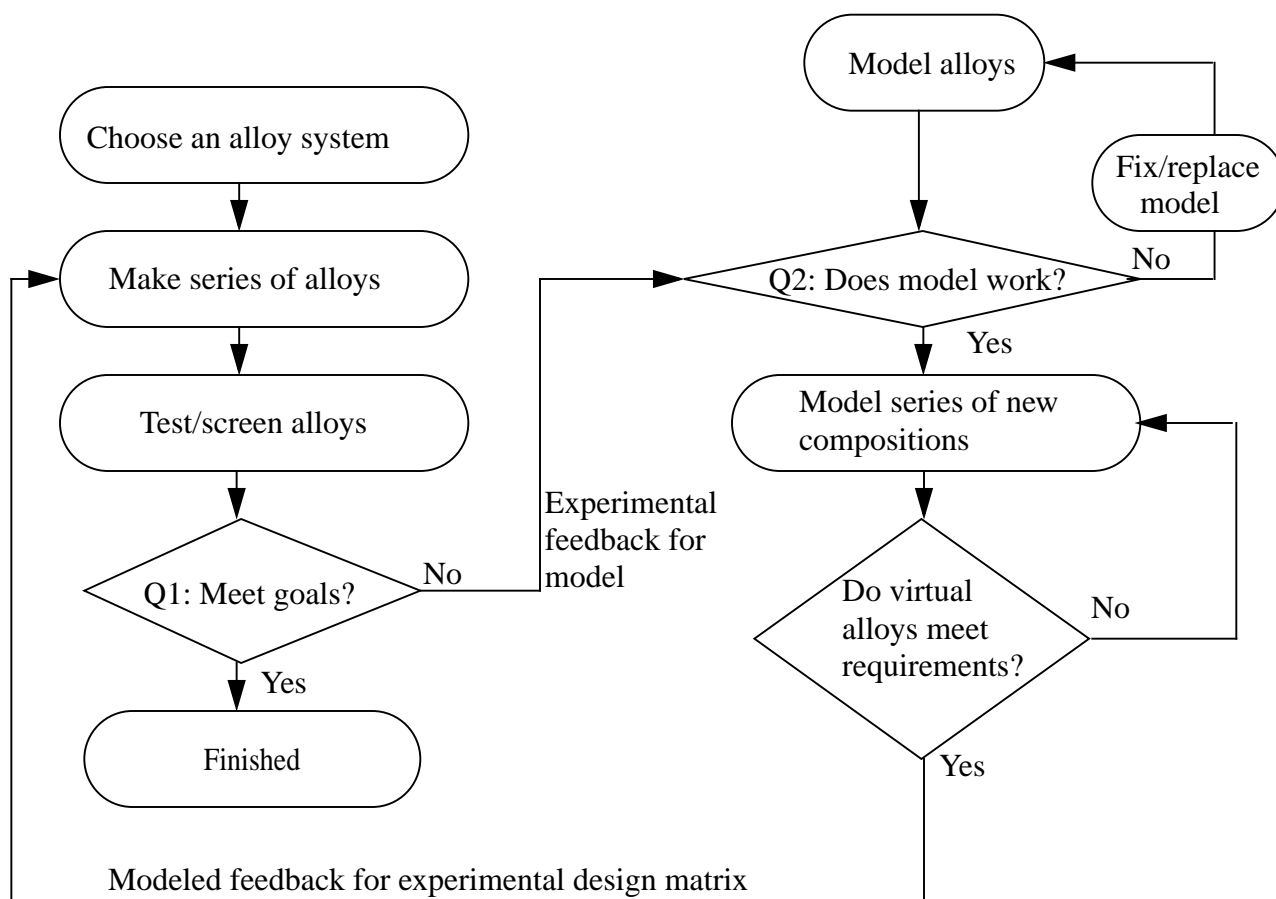


Figure 1.b Integrated Alloy Design Program with Mutual Feedback



the rate and resource limiting step.

This paper represents the first in the series of articles detailing our design program on NiAl-based alloys. In forthcoming papers, we will describe our experimental and theoretical investigation of a series of 3-, 4- and 5-element alloys based on NiAl, highlighting the connection between the two approaches. In this first paper we will provide a detailed description of the BFS method and use it to reproduce the basic features of the base material, with as much accuracy as possible, since the forthcoming extension of the model to complex systems will rely only on our ability to describe the most basic system.

Therefore we will initially concentrate on the  $\beta$ -phase of the binary Ni-Al system, which exists over a range of stoichiometry from about 45-60 at. % Ni [4]. At the stoichiometric composition NiAl should exist in a perfectly ordered state where the Ni atoms occupy the cube corners and the Al atoms occupy the cube centers of a generalized body-centered cubic lattice. Ni-rich alloys are characterized by antisite point defects, where Ni atoms occupy sites in the Al sublattice, resulting in a decrease in lattice parameter and an increase in density with increasing Ni content. A different behavior is observed on the Al-rich side of stoichiometry. There is a steep decrease in lattice parameter as well as a greater than expected decrease in density with increasing Al content. The presence of vacancies in Ni sites would explain such behavior [4-8]. Recent X-ray diffraction experiments [9] suggest a richer structure: the evidence, while strongly favoring the presence of vacancies in Ni sites, also suggests the possibility of some vacancies in Al sites in a 3:1 ratio. Moreover, local ordering of vacancies may be preferred over a random distribution of individual point defects [6].

While some of the concepts introduced in this first paper might seem too detailed for the task at hand (i.e. describing the defect structure of  $\beta$ -NiAl), they will be strictly necessary for a full

understanding of the results from more complex systems that will appear in subsequent papers in this series. In other words, we are establishing the validity of our model by eliciting a positive response to ‘Q2’ in Fig. 1.b before proceeding further along the flow chart.

In most cases, theoretical techniques at the atomic level are used for validating or understanding experimental findings, a task somewhat removed from the actual process of alloy design. In this series, we embark on a process of materials development starting with the validation of our theoretical approach with established experimental knowledge of the basic, binary system (this first paper), building on our theoretical predictions as the complexity of the system increases (ternary, quaternary alloys), finally allowing us to determine the structural properties of a 5-element alloy (last paper) based on this groundwork. As a whole, this series of papers is meant to prove another point, which goes beyond the features of the particular problems at hand: that semiempirical methods, tied to powerful numerical techniques and implemented in the framework of an economical and easy to handle operational procedure, can constitute a very useful tool in effectively aiding in the area of materials design.

This paper introduces, in detail, the BFS method and its operational equations. After introducing the novel way of partitioning the alloy formation process proposed by the BFS method and conceptually defining the quantities of relevance, we present details of the operational procedure. We continue with an example illustrating the implementation of the method. As a consequence of the tremendous advance in semiempirical techniques over the last decade, we conclude this section with a brief description of recent work done with other techniques of comparable complexity as well as their relation to BFS. We continue by introducing the computational scheme chosen to address the structure of NiAl, a procedure which will be used and expanded in subsequent papers dealing with higher order alloys. We conclude by providing the BFS predictions for the defect

structure and physical properties of  $\beta$ -NiAl, comparing them with experimental results when possible, thus providing us with confidence in our model.

## THE BFS METHOD

The BFS method is one of the latest additions to the growing family of quantum-mechanical, approximate techniques for the calculation of materials properties. It has a strong foundation in quantum theory, but simplifies the numerical effort usually associated with ab-initio methods. While a great deal of detail (i.e. electronic structure) is lost when applying semiempirical methods to specific systems, valuable insight on the general behavior of physical systems is gained, since the simplicity of the formulation allows for a quick and sufficiently accurate estimate of general properties.

Several methods successfully deal with single-element metallic systems, providing a wealth of information on their physical properties and defect structures [10-15]. However, in the case of extended defects, i.e. surfaces, some methods exhibit limitations in their predictive power [11]. In most cases the corresponding potentials or the parameters used in the algorithm, are usually determined from bulk properties and are therefore limited in their ability to properly reproduce these defects. However, the overall power of semiempirical techniques has enabled a better understanding of defects such as surface phenomena in spite of these shortcomings, which has led to extensive growth in the area of computer simulations of defects.

For alloy structures, semiempirical methods have been less effective in providing results with the same degree of reliability as those for single-element systems. This is partly due to the nature of the formalisms. Either an impractical number of parameters is needed (modified embedded

atom method [11] and tight-binding methods [12], for example) or specific potentials have to be determined on a case-by-case basis to deal with each specific alloy composition or phase, therefore limiting their transferrability.

In spite of these limitations, there has been remarkable progress in the last few years. In combination with the development of powerful first-principles methods and an ever increasing computational power, theoretical approaches are becoming tools of great value for understanding, modeling and designing materials suited for industrial applications.

Perhaps the main contribution of the BFS method to the field of computationally oriented semiempirical methods, is that it is basically free of most of the restrictions that limit the application of comparable techniques [16]: there is no restriction on crystal structure or the type of atomic species considered and the number of input parameters is reduced to a minimum. Moreover, no experimental input is necessary, as all the input parameters can be determined by simple first-principles calculations [17].

These advantages of the BFS method make it particularly suitable for broad alloy design problems where the nature of the predictions is comparable to the information that can be obtained from experimental analysis (in this work, for example, we attempt to study the structure of 5-element alloys, both theoretically and experimentally). It is precisely this issue that motivates the present work: to develop a reasonably accurate and computationally simple theoretical approach that can provide valuable input for the development of new materials, in close conjunction with experiment.

Since its inception a few years ago [18], the BFS method has been successfully applied to a variety of situations ranging from segregation profiles [16], alloy structure [19], surface alloying of immiscible metals [20], to numerical simulations of the scanning tunneling microscopy tip-

sample interaction [21], bulk alloy design [1,22] and alloy surface structure [23]. Two of the characteristics of the early applications of the BFS method, i.e., the need for experimentally determined input data and complete reliance on the pure constituent properties [18], initially imposed a limitation when dealing with systems like  $\beta$ -NiAl, where both constituents are fcc elements but the alloy is bcc-based. No appropriate experimental input for bcc-Ni and Al is available. Therefore, as shown in detail later in this work, we have reformulated the method relying only on pure first-principles determined input, thus freeing BFS from limitations imposed by the restricted availability of experimental data. We also avoid the potential problem of inconsistency or inaccurate data obtained from different experimental techniques [14]. While the method retains the same operational algorithm used in its previous applications, the new parameterization scheme presented in this paper greatly enhances its range of applications and accuracy.

### *General concepts*

The BFS method provides a simple algorithm for the calculation of the energy of formation  $\Delta H$  of an arbitrary alloy (i.e. the difference between the energy of the alloy and that of its individual constituents). In BFS, the energy of formation is written as the superposition of individual contributions of all the atoms in the alloy,

$$\Delta H = \sum_i (E'_i - E_i) = \sum_i e_i \quad (1)$$

where  $E'_i$  is the energy of atom  $i$  in the alloy and  $E_i$  its corresponding value in a pure equilibrium monatomic crystal. In principle, the calculation of  $\Delta H$  would simply imply computing the energy

of each atom in its equilibrium pure crystal and then its energy in the alloy. In BFS, beyond directly computing the difference  $e_i$  for each atom in the alloy, we introduce a two-step approach for such a calculation in order to identify contributions to the energy due to structural and compositional effects. Therefore, we break up the individual contributions of each atom  $e_i$  to the total energy of formation  $\Delta H$  of the sample into two components: a strain energy and a chemical energy.

While there is a certain level of arbitrariness in how this separation is implemented, it is only meaningful when a good representation of the actual process is obtained by properly linking both contributions. In other words, a proper coupling of these two apparently independent processes (strain and chemical effects) must be accomplished in order for the final result to approach the result one would obtain if a straightforward calculation (i.e. ab-initio methods) was carried out.

We define the BFS strain energy as the contribution to the energy of formation from an atom in an alloy computed as if all the surrounding atoms were of the same atomic species, while main-

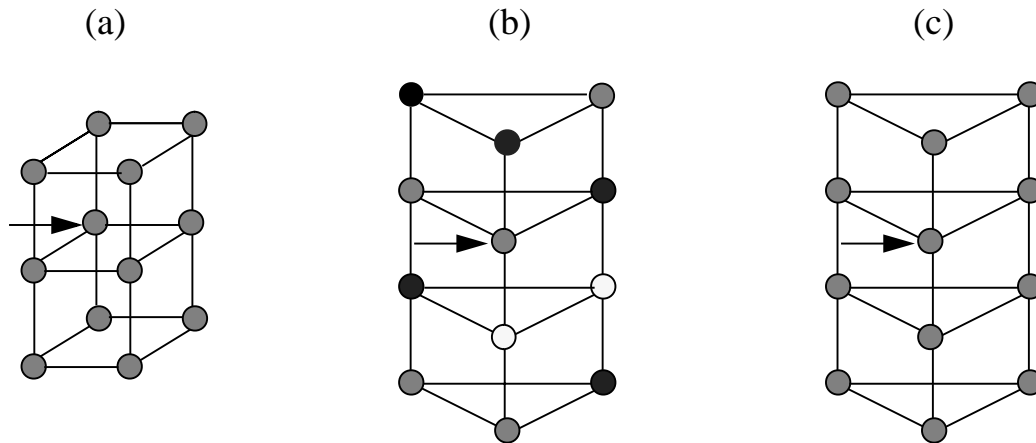


Fig 2: (a) A pure, equilibrium crystal (reference atom denoted by the arrow), (b) a reference atom (denoted by the arrow) in the alloy to be studied (atoms of other species denoted with other shading) and (c) the same reference atom in a monatomic crystal, with the identical structure of the alloy to be studied, but with all the atoms of the same atomic species as the reference atom, for the calculation of the strain energy term for the reference atom. The strain energy is the difference in energy of the reference atom between (c) and (a).

taining the original structure of the alloy. To visualize this concept, Fig. 2.a represents the atom in question (identified with an arrow) in an equilibrium position in its ground state crystal (arbitrarily represented by a simple cubic lattice). Fig. 2.b shows the same atom in the alloy being studied (also arbitrarily represented by a different crystallographic symmetry). Two things can be different between the reference crystal and our alloy. First, atoms of other species may occupy neighboring sites in the crystal and second, the crystal lattice may not be equivalent in size or structure to that of the ground state crystal of the reference atom. In Fig. 2.b, the different atomic species are denoted with different symbols from that used for the reference atom, and the differences in size and/or structure are denoted with a schematically different atomic distribution as compared to the ground state crystal shown in Fig. 2.a. The BFS strain energy term accounts for the change in energy due *only* to the change in the geometrical environment of the crystal lattice (from 2.a to 2.b), ignoring the additional degree of freedom introduced by the varying atomic species in the alloy. In this context, Figure 2.c shows the environment ‘seen’ by the reference atom when computing its BFS strain energy contribution. The neighboring atoms conserve the sites in the actual alloy (fig. 2.b), but their chemical identity has changed to that of the reference atom (fig. 2.a), thus simplifying the calculation to that of a single-element crystal. The BFS strain energy term represents the change in energy of the reference atom in going from the configuration denoted in Fig. 2.a to Fig. 2.c.

This choice for the BFS strain energy introduces two main advantages. First, by transforming (for each atom) the actual alloy into a monatomic crystal, it greatly simplifies the calculation of the energy of the reference atom in the alloy structure, making it amenable to a large number of theoretical techniques that can efficiently deal with this simplified situation. Second, it gives partial information concerning *only* the structure of the alloy, which could serve later to identify fine

geometrical effects on structure.

The second contribution to the BFS energy of formation is the chemical energy. Here, we are interested in isolating the effect of compositionally different atoms occupying neighboring sites to the reference atom. In order to do this, we leave out any structural information from the original lattice by *forcing the neighboring atoms to occupy equilibrium lattice sites corresponding to sites in the pure cell of the reference atom*, changing the composition of the atoms to match the chemical profile in the alloy lattice. Fig. 3.a shows the reference atom in the actual alloy (similar to Fig. 2.b), while Fig. 3.b indicates the atomic distribution used in computing the BFS chemical energy (note that the lattice used in Fig. 3.b corresponds to that of the ground state crystal of the reference atom as shown in Fig. 2.a).

The chemical energy is then based on the difference between the energy of the reference atom in Fig. 3.b and its energy in its ground state crystal (Fig. 2.a). In order to completely free the chemical energy from structural defects, certain provisions have to be made which will be clearly

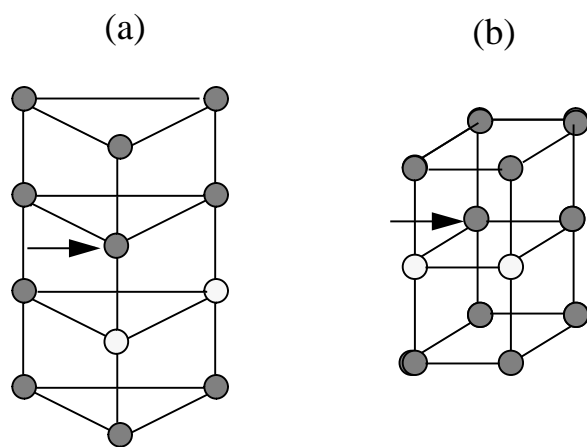


Fig. 3: (a) The reference atom (denoted by an arrow) in the actual alloy environment and (b) the reference atom surrounded by a chemical environment equivalent to that in (a) but with the different neighboring atoms occupying equilibrium lattice sites corresponding to the ground state of the reference atom.



detailed later in this section.

So far, we have exploited the flexibility in partitioning the energy of formation to provide ourselves with a simple and straightforward framework for computing both the BFS strain and the BFS chemical energy contributions. However, a simple addition of these two quantities does not necessarily constitute a good approximation to the actual energy of formation. After decoupling the structural and chemical processes involved in alloy formation, we now recouple them by introducing a coupling function which, in its definition, has the necessary ingredients to ensure that this partitioning scheme accurately reproduces a full calculation of the energy of formation when recombined in this manner. The definition of the coupling function will be clear once we introduce the necessary tools for computing the individual (strain and chemical) contributions in the following subsections. We therefore write the energy of formation of the alloy as

$$\Delta H = \sum e = \sum (e_S + g e_C) \quad (2)$$

where  $e_S$  is the strain energy,  $e_C$  is the chemical energy,  $g$  is the coupling function and the sum extends over every atom in the alloy.

### *Strain energy*

The actual calculation of the BFS strain energy for each atom is straightforward and any technique designed to compute the energetics of pure crystals should be appropriate. However, in spite of the apparent simplicity of this task, few techniques are actually capable of performing it successfully in general situations. The choice should be limited to only those techniques that intro-

duce a substantial level of accuracy, regardless of the geometry of the environment, as well as those characterized by straightforward numerical determination. While first-principles calculations would be ideal for performing this task, they are still limited by the excessive computational effort associated with complex geometries. It is true that because of the simplicity of the NiAl case, first-principles techniques could be used without major difficulties. However, this might not be true when multiple alloying additions are considered. On the other hand, the computational effort involved is not an issue with other semiempirical techniques comparable to BFS, but most still fail in properly dealing with this situation in the presence of extended defects from a physical standpoint or by relying heavily on parameters that might not be applicable or effective for the type of alloy structure under consideration.

In all previous applications of BFS, we have used the Equivalent Crystal Theory (ECT) [24,25], which in a straightforward manner, provides a simple algorithm for the calculation of defect energies even in the presence of such radical defects as surfaces. The underlying concept of ECT is simple and clear and it becomes particularly easy to understand if presented in terms of the Universal Binding Energy Relation (UBER) [26]. Consider the ground state crystal, characterized by the equilibrium value of the Wigner-Seitz cell,  $r_{\text{WSE}}$ . An isotropic expansion or compression of such a crystal from its equilibrium shape (where all bonds are expanded or compressed equally in all directions) yields a universal (in the sense that it has the same shape for all elements) curve for the energy vs. Wigner-Seitz radius (or atomic volume), as shown in Fig. 4.a.

If the reference atom is in an equilibrium position in the ground state crystal, it sits at the bottom of this curve, with an energy  $-E_c$  (cohesive energy). If this crystal is deformed anisotropically, or if a defect is introduced in the vicinity of the reference atom (i.e., a vacancy, an interstitial atom, etc.), it raises its energy. The curve indicates that there are two values of the Wigner-Seitz

radius for which each atom in a homogenous, ideal, crystal have the same energy as the reference atom in the defect crystal. We will call these two crystals, *equivalent crystals* of the reference atom. These two positions represent two different conditions. To the right of the minimum the crystal has an increased lattice parameter and thus a reduced electron density. To the left of the minimum the opposite is true.

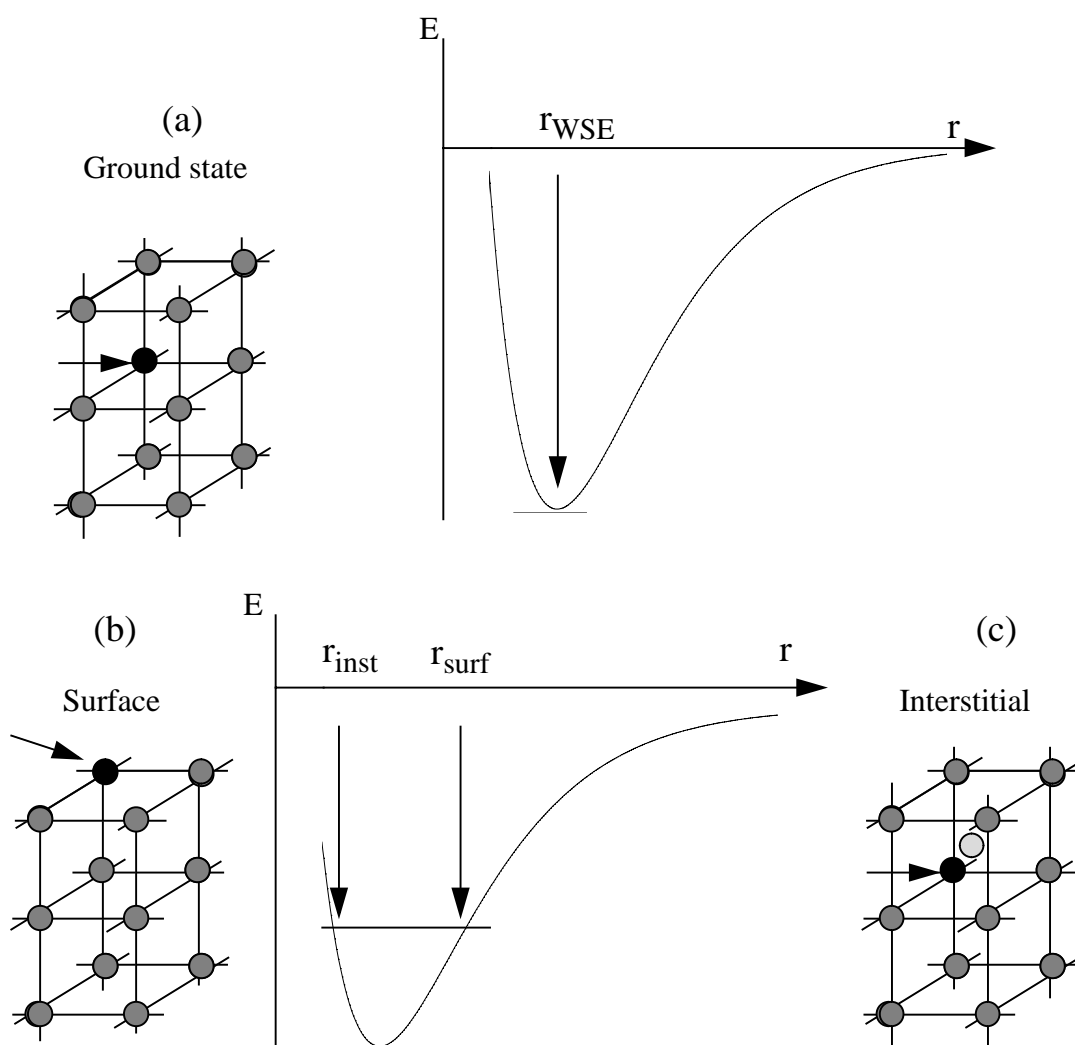


Fig. 4: Universal binding energy relation (E vs. r) for a monatomic crystal. When all atoms are in their equilibrium lattice sites, the energy of each atom is the cohesive energy, indicated with the arrow in (a). In the presence of a surface (b) or in the presence of an interstitial atom (c), a given atom will have a higher energy along the binding energy curve, which also corresponds to a certain ideal perfect crystal with an expanded (b) or compressed (c) lattice parameter. Any atom in these equivalent crystals have the same energy as those of the reference atoms (denoted by an arrow) in (b) and (c).

For example, an atom on the surface of a metal (Fig. 4.b), after losing a large number of neighbors, thus increasing its energy substantially due to the decrease in electron density, has the same energy in that situation that it would have in a perfect crystal but with a larger lattice parameter. In terms of its *energy*, the atom would not distinguish between being on the surface or being in a larger version of the ground state crystal. Conversely, if an interstitial atom is introduced close to the reference atom, its energy increases to an amount equivalent to the one that it would have in a properly homogeneously compressed ideal crystal. Figure 5 reiterates these concepts, showing the equivalent crystals of a surface atom. As a consequence, every point along the UBER of a certain crystal is degenerate, as there is a large number of defects that would have the same energy, and therefore, the same equivalent crystal. In other words, the reference atom can find itself in the presence of a number of different defects that raise its energy by the same amount, therefore assigning the same equivalent crystal to all those defects.

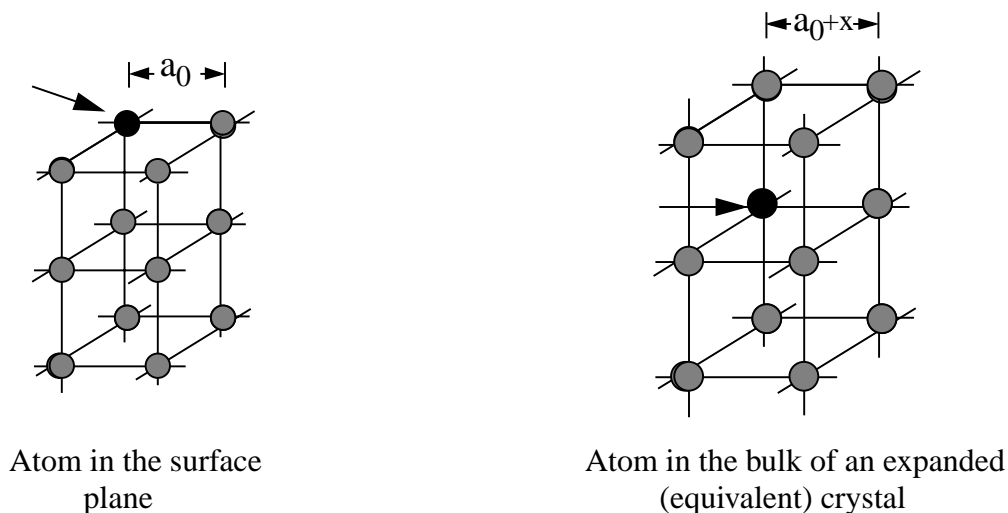


Figure 5: Equivalent crystals of a surface atom. The surface atom is in an environment of reduced electron density, equivalent to that found in an isotropically expanded bulk crystal.

ECT provides an efficient algorithm for finding the equivalent crystal for each atom, corresponding to a certain environment, based on quantum perturbation theory. We refer the reader to Ref. 24 for a derivation of the ECT equations from perturbation theory, and to Ref. 25 for more details on the implementation of the ECT operational equations. Once the reference atom is chosen, all that is needed is to know the distances between the reference atoms and a group of its neighbors. Although no preset cut-off distance is defined in ECT, it is sufficient in most cases to consider all neighbors up to second or sometimes third-neighbor distances. Finding the equivalent crystal for a certain atom near a defect translates into finding the equivalent lattice parameter, i.e., the expanded or compressed lattice parameter of the equivalent crystal, such that the energy of an atom in that crystal is the same as that of the atom in the defect crystal. This is done by solving the following transcendental equation for the lattice parameter of the equivalent crystal (see Ref. 24 for a detailed derivation of this equation)

$$NR_1^p e^{-\alpha R_1} + MR_2^p e^{-\left(\alpha + \frac{1}{\lambda}\right)R_2} = \sum_k r_k^p e^{-(\alpha + S(r_k))r_k} \quad (3)$$

where  $N$  and  $M$  are the ideal number of nearest-neighbors ( $N$ ) and next-nearest neighbors ( $M$ ) in the equivalent (ideal) crystal,  $R_1$  and  $R_2$  are the nearest-neighbor and next-nearest-neighbor distances, respectively, in the equivalent crystal, and where  $p$ ,  $\alpha$  and  $l$  are ECT parameters that fully describe the corresponding atomic species within the context of ECT [24]. Eq. 3 is solved for  $a_S$ , the lattice parameter of the equivalent crystal ( $R_1$  and  $R_2$  are the nearest neighbor and next nearest neighbor distances, respectively, in a crystal with lattice parameter  $a_S$ ). The right hand side (r.h.s.) of this equation, which is computed in terms of the actual distances for the known structure in the defect crystal  $r_k$ , can be interpreted as a measure of the defect (in the sense of how the actual envi-

ronment surrounding the reference atom differs from that in its pure crystal) due to the actual atomic environment of the reference atom where  $r_k$  are the distances between these atoms and the reference atom.  $S(r)$  is a screening function, also to be defined later. The sum runs over all neighboring atoms (at distances  $r_k$ ) within a sphere of radius  $r_c$ , defined as the next-nearest neighbor distance in the perfect equilibrium lattice.

If this equation admits a solution, that means that the equivalent crystal associated with the reference atom is properly defined and its energy can be determined by use of the binding energy relationship (demonstrated to accurately represent the UBER) [25,26]:

$$e_S = -E_c(1 + a_S^*)e^{-a_S^*} \quad (4)$$

The scaled lattice parameter  $a_S^*$  is related to the solution of Eq. 3,  $a_S$ , by means of the following expression

$$a_S^* = q \frac{(a_S - a_e)}{l} \quad (5)$$

where  $a_e$  is the equilibrium lattice parameter,  $E_c$  is the cohesive energy of the ground state crystal,  $q$  is the ratio between the equilibrium lattice parameter and the equilibrium Wigner-Seitz radius  $r_{WSE}$ , and  $l$  is a scaling length to be defined later. Having computed the equivalent crystal, we now determine the BFS strain energy contribution of the reference atom as the difference between the energy of the atom in the defect crystal and its energy at equilibrium in its ground state crystal:

$$e_S = E_c \left( 1 - (1 + a_S^*)e^{-a_S^*} \right) \quad (6)$$

where the subindex  $S$  to the scaled lattice parameter denotes the fact that this equivalent crystal is related to the strain energy component of this atom in the alloy. The parameters  $p$ ,  $\alpha$ ,  $l$  and  $\lambda$  are ECT parameters that fully describe the atomic species in question:  $p$  is  $2n-2$ , where  $n$  is the principal quantum number,  $a_e$  is the equilibrium lattice parameter,  $l$  is a scaling length and  $\lambda$  is a screening factor to properly account for screening effects beyond first neighbors (see Ref. 24 for a full description of the determination of these parameters).

The parameter  $\alpha$ , which is directly related to the structure of the wave function in the overlap region between similar atoms, has been determined in past applications of ECT by requiring that the formalism reproduces the experimental value of the single vacancy formation energy [24,25]. However, in order to minimize the dependence on experimental or theoretical input for the determination of these parameters, we now introduce a novel way of determining the parameter  $\alpha$ , which provides the additional benefit of determining the range of validity of the approximations introduced in writing the perturbation equation for the calculation of the equivalent crystal. As mentioned before, the r.h.s. of Eq. 3 can be considered as a ‘measure’ of the defect (in the sense that the departure of this quantity from its equilibrium value is representative of the difference between the defect crystal and the perfect, equilibrium crystal). For example, the presence of vacancies close to the reference atom reduces the value of this quantity, while other defects, like interstitials, increase its value. While a solution exists for arbitrarily small values of this quantity, this is not so for values much larger than the one corresponding to equilibrium (for which the equivalent crystal is the equilibrium crystal itself). There is a maximum value for the r.h.s of Eq. 3 above which no solution to this equation can be found. We therefore determine  $\alpha$  by requiring that this maximum defect corresponds to the situation when the strain energy of the reference atom equals its cohesive energy. In doing so,  $\alpha$  becomes dependent on the other parameters characteriz-

ing the atomic species ( $E_c$ ,  $a_e$ ,  $p$ ,  $l$ ,  $\lambda$ ). This redefinition of the ECT parameter  $\alpha$  reduces the actual necessary input to just the cohesive energy ( $E_c$ ), the equilibrium lattice parameter ( $a_e$ ), and the bulk modulus ( $B_0$ ) since  $l$  is directly related to these three parameters by

$$l^2 = \frac{E_c}{12\pi r_{WSE} B_0} \quad (7)$$

where  $r_{WSE}$  denotes the equilibrium value of the Wigner-Seitz radius. Furthermore, the screening length  $\lambda$  [24] is defined as

TABLE 1  
COMPUTED INPUT PARAMETERS FOR NiAl CALCULATIONS

LMTO results				
Atom	Lattice Parameter $a_e$ (Å)	Cohesive Energy $E_c$ (eV)	Bulk Modulus $B_0$ (GPa)	Vacancy Energy $E_v$ (eV)
Ni	2.752	5.869	249	3.0
Al	3.190	3.942	78	1.8
ECT parameters				
Atom	$p$	$\alpha$ (Å <sup>-1</sup> )	$l$ (Å)	$\lambda$ (Å)
Ni	6	3.067	0.763	0.2717
Al	4	1.8756	1.038	0.3695
BFS parameters				
$\Delta_{\text{NiAl}} = -0.0581 \text{ Å}^{-1}$ $\Delta_{\text{AlNi}} = 0.0840 \text{ Å}^{-1}$				

LMTO results and ECT parameters for bcc-based Ni and Al, and BFS parameters for B2 NiAl.



$$\lambda = 2.81l. \quad (8)$$

Finally, the screening function  $S(r)$  is defined by  $S(r)=0$  if  $r < r_1$ ,  $S(r) = (1/2\lambda)(1 - \cos \beta)$  if  $r_1 < r < r_2$  (where  $\beta = \pi(r-r_1)/(r_2-r_1)$ ) and  $S(r) = 1/\lambda$  if  $r > r_2$ , where  $r_1$  and  $r_2$  are the equilibrium nearest- and next-nearest-neighbor distances in the equilibrium crystal [24,25].

### *Chemical energy*

The calculation of the chemical energy involves an environment related to the ground state of the reference atom (i.e., the reference atom, as well as its neighbors, are located in equilibrium lattice sites corresponding to the ground state crystal of the reference atom) although the actual chemical distribution of the atoms is conserved. Given the actual chemical environment of a given atom (those atoms within next-nearest neighbor distance from it), it is straightforward to determine an equivalent chemical environment in a perfect crystal. A set of transformations can be defined which assigns, to each site in the perfect crystal, the appropriate chemical species. The resulting distribution is then chemically equivalent to that found in the alloy. In essence, the same considerations made for the strain energy apply here, with the only difference being that the changes of electron density in the vicinity of the reference atom are now due to changes in the atomic identity of the neighboring atoms rather than changes in the atomic locations. In this sense, the same concepts (the existence of an equivalent crystal) apply, only now the reference atom can have different energies than that allowed by its own UBER. As mentioned before,  $\alpha$  is the only parameter within our formalism that carries all the information regarding the electron density in the overlap region between a pair of atoms. For dissimilar atoms it is only natural then to ‘perturb’

such an environment by allowing the wave function in that region to be parameterized by a slightly different parameter than that used in monatomic calculations. We therefore define the BFS parameter  $\Delta_{AB}$  (and  $\Delta_{BA}$ ), given by

$$\alpha_{AB} = \alpha_A + \Delta_{BA} \quad (9)$$

when the reference atom is of species A and its neighbor of species B and

$$\alpha_{BA} = \alpha_B + \Delta_{AB} \quad (10)$$

when B is the reference atom and its neighbor is an A atom. The BFS parameter  $\Delta_{AB}$  (or  $\Delta_{BA}$ ) perturbs the pure element parameter  $\alpha$ , indicating the mixed nature of the bond.

Following the guidelines for writing Eq. 3 and taking into account that the neighboring atoms are by definition located in equilibrium lattice sites of the reference atom, the transcendental equation to be solved for the (chemical) equivalent crystal is simply

$$NR_1^{p_A} e^{-\alpha_A R_1} + MR_2^{p_A} e^{-\left(\alpha_A + \frac{1}{\lambda_A}\right)R_2} = \sum_k r_{1,A}^{p_A} e^{-(\alpha_A + \Delta_{kA})r_{1,A}} + \sum_k r_{2,A}^{p_A} e^{-\left(\alpha_A + \Delta_{kA} + \frac{1}{\lambda_A}\right)r_{2,A}} \quad (11)$$

where  $r_{1,A}$  denotes the nearest neighbor distance in an ideal crystal A and  $r_{2,A}$  the corresponding next-nearest neighbor distance. All other terms have their previous meanings. The calculation of the chemical energy proceeds from solving Eq. 11 for  $a_c$ , the lattice parameter of the equivalent crystal for which  $R_1$  and  $R_2$  are the nearest- and next-nearest neighbor distances, respectively, and then determining the scaled lattice parameter  $a_c^*$  given by

$$a_C^* = q \frac{(a_C - a_A)}{l_A} \quad (12)$$

so that the chemical energy is

$$e_C = \gamma E_c \left( 1 - (1 + a_c^*) e^{-a_c^*} \right) \quad (13)$$

where  $\gamma = 1$  if  $a_c^* > 0$  and  $\gamma = -1$  if  $a_c^* < 0$  [18].

Finally, a safeguard should be introduced in the definition of the chemical energy contribution to account for those situations where the reference atom does not have full coordination (i.e., the number of nearest-neighbors is less than that found in the perfect, equilibrium crystal). Consider the reference atom occupying a surface site of an alloy. In computing the chemical energy, information about the existence of the surface is introduced by the fact that there are not enough atoms in the vicinity of the reference atom to correspond to the assumption in Eq. 11. The chemical energy obtained in this way would carry information not only on the chemical effect but also on the structural effect due to the absence of some neighbors. In order to completely free the chemical energy from this structural information, we reference the previously defined chemical energy to a similar structural state but where all the atoms surrounding the reference atom are of the same identity as the reference atom. A reference chemical energy  $e_{C_0}$  is thus computed in this manner, so that the total chemical energy contribution from the reference atom is

$$\varepsilon_C = e_C - e_{C_0}. \quad (14)$$

where  $e_{C_0}$  is computed using Eq. 11 but setting the BFS parameters to zero. The energy is then computed using Eqs. 12 and 13.

### *Coupling the strain and chemical energy*

As defined, the chemical energy does not depend on the actual geometry of the alloy which is, obviously, unrealistic. Therefore the BFS strain and chemical energy terms need to be recoupled by properly accounting for the influence of structural effects on the chemical contribution. In order to properly describe the asymptotic behavior of such a quantity ( $\epsilon_C$  should vanish at large separations and should drastically increase at small separations), we introduce a coupling function  $g$  linking both terms. The coupling function introduces this asymptotic dependence by means of  $a_s^*$ , the strain scaled lattice parameter (Eq. 5), which can be understood as a measure of the strain effect. If  $a_s^* = 0$  it means that the reference atom finds itself in an environment that resembles equilibrium; a positive value of  $a_s^*$  results from average expansions with respect to equilibrium and negative values of  $a_s^*$  relate to average compressions. We therefore define the coupling function  $g$  as:

$$g = e^{-a_s^*} \quad (15)$$

so that defects that involve expansions reduce the effect of the chemical energy on the total energy of formation and viceversa. Fig. 6 displays the effect of the coupling function  $g$  on the chemical energy, which otherwise would amount to a constant contribution to  $\Delta H$ , independent of the size of the cell. Summarizing these concepts, the BFS contribution  $e$  from an atom  $i$  to the energy of formation  $\Delta H$  is given by

$$e = e_S + g(e_C - e_{C_0}) = e_S + g\epsilon_C \quad (16)$$

A graphical representation of the calculation of  $e$  is shown in Fig. 7.

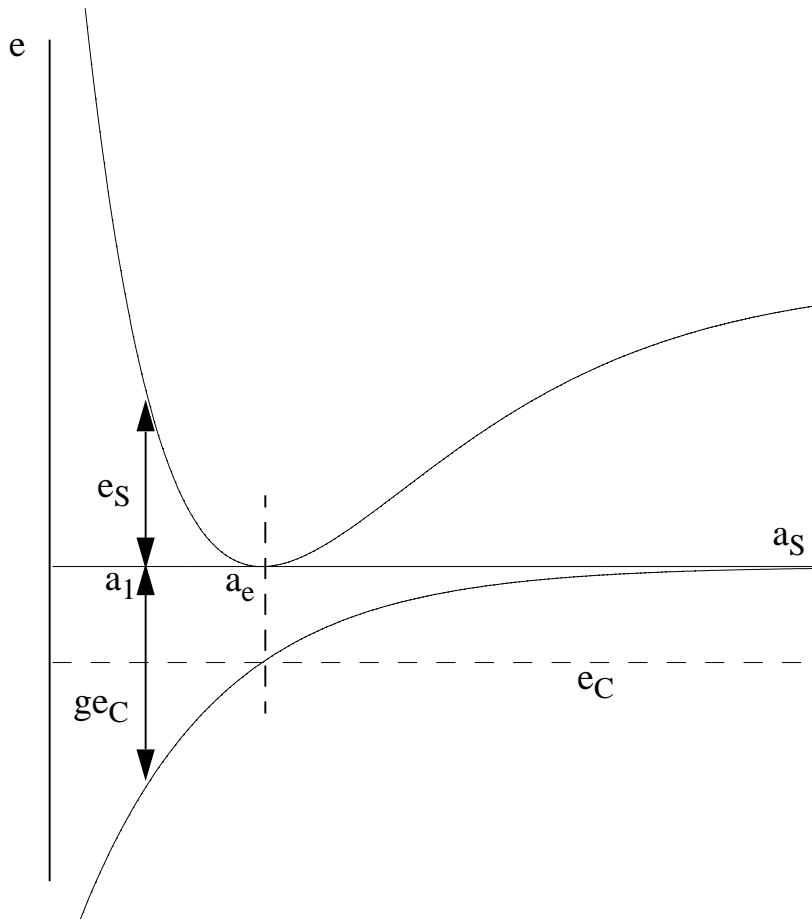


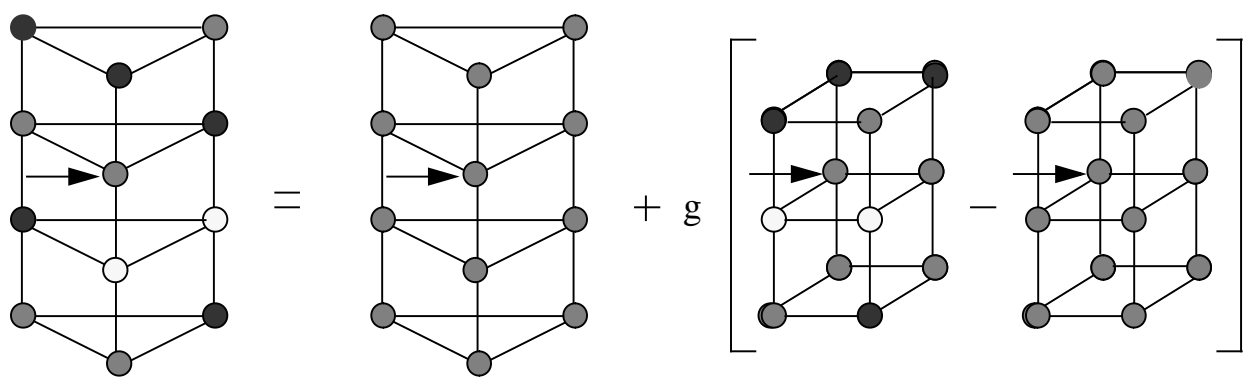
Fig. 6: Schematic representation of the strain and chemical energy contributions of an atom A in an alloy as a function of the (strain) equivalent lattice parameter  $a_s$ . The dashed line indicates the constant value of the chemical energy, which amounts to the total contribution to the energy of formation only when the lattice parameter of the alloy coincides with that of the equilibrium crystal A. The total chemical energy contribution,  $ge_C$ , vanishes at large interatomic separations. For example, if the equivalent (strain) lattice parameter is  $a_1$ , we show the corresponding strain ( $e_s$ ) and chemical ( $ge_C$ ) energy contributions. If the equivalent (strain) lattice parameter is  $a_e$ , then  $e_s = 0$  and  $e_C$  corresponds to its constant value ( $g = 1$ ).

### *Applying BFS to the calculation of the energy of formation of a bcc binary alloy*

To demonstrate the ideas presented thus far, we apply the BFS formalism to the calculation of the energy of formation of a binary A-B alloy in the B2 structure, as a function of the alloy lattice parameter  $a_0$ . Fig. 8 represents the alloy formation process where two pure bcc crystals A and B, each with equilibrium lattice parameters  $a_A$  and  $a_B$  are reassembled to form a B2 alloy with lattice parameter  $a_0$ . In the absence of defects, this is a particularly simple example due to its high symmetry and uniformity. All A atoms are equivalent, and so are the B atoms. It is only necessary to

compute the energy contribution of one generic A atom and one B atom. In what follows, we will compute  $e_A$  only, since  $e_B$  would be computed in the same manner. The different contributions to  $e_A$  are shown in Fig. 9.

In writing the equation for the calculation of the BFS strain energy (see Eq. 3), we note that in the actual alloy an A atom has 8 nearest neighbor B atoms at a distance  $r_I$  and 6 next-nearest neighbor A atoms at a distance  $a_0$ . Following the method for evaluating the strain energy environment, we must remember to ‘flip’ the identity of these neighbors to that of the reference atom. The BFS strain energy equation for atom A is then

$$e = e_s + g ( e_C - e_{C_0} )$$


The diagram illustrates the components of the BFS energy equation. On the left, a 3D lattice structure shows a reference atom (white circle) with an arrow pointing to it. This is equated to the strain energy term  $e_s$ , which shows the same lattice with atoms of the same species as the reference atom in their actual positions. This is then added to the term  $g(e_C - e_{C_0})$ , where  $e_C$  represents the chemical energy term (atoms in ideal lattice sites) and  $e_{C_0}$  represents the reference chemical energy (atoms retaining the original identity of the reference atoms).

Fig. 7: Schematic representation of the BFS contributions to the total energy of formation. The left hand side represents the reference atom (denoted by an arrow) in an alloy. The different terms on the right hand side indicate the strain energy (atoms in their actual positions but of the same atomic species as the reference atom), the chemical energy term (atoms in ideal lattice sites) and the reference chemical energy (same as before, but with the atoms retaining the original identity of the reference atoms).

$$8R_1^{p_A} e^{-\alpha_A R_1} + 6R_2^{p_A} e^{-\left(\alpha_A + \frac{1}{\lambda_A}\right)R_2} = 8r_1^{p_A} e^{-\alpha_A r_1} + 6a_0^{p_A} e^{-\left(\alpha_A + \frac{1}{\lambda_A}\right)a_0} \quad (17)$$

This equation is trivially solved, with the lattice parameter of the equivalent crystal being just  $a_S^A = a_0$ . The corresponding BFS strain energy contribution is

$$e_S^A = E_c^A \left( 1 + (1 + a_S^{A*}) e^{-a_s^{A*}} \right) \quad (18)$$

where the scaled lattice parameter of the (strain) equivalent crystal is given by

$$a_S^{A*} = q \frac{(a_0 - a_A)}{l_A}. \quad (19)$$

A similar calculation is carried out for atom B, replacing  $p_A$ ,  $l_A$ ,  $a_A$  and  $\lambda_A$  with  $p_B$ ,  $l_B$ ,  $a_B$  and  $\lambda_B$  in Eqs. 17-19. From the calculation of the strain energy contributions for atoms A and B one

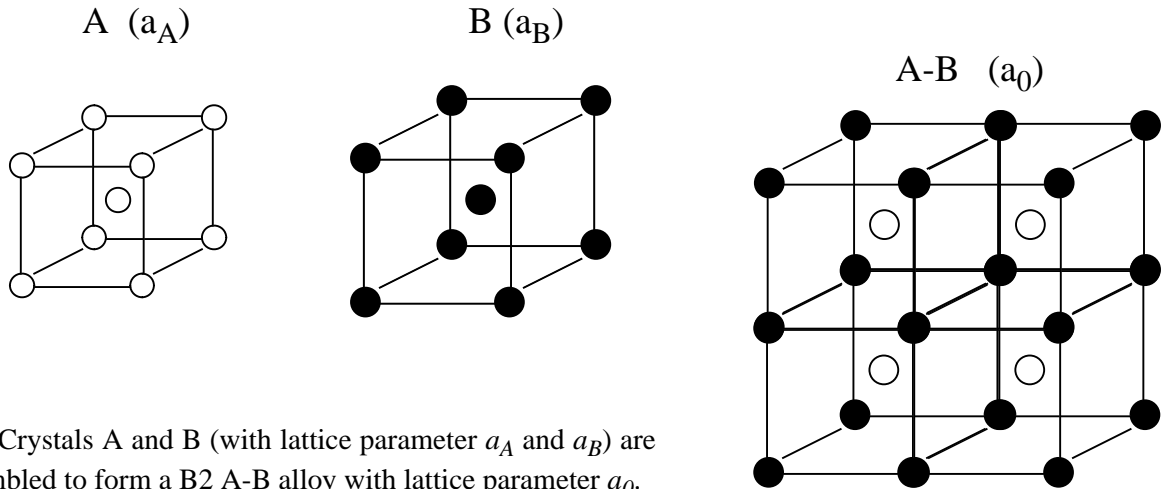


Fig. 8: Crystals A and B (with lattice parameter  $a_A$  and  $a_B$ ) are reassembled to form a B2 A-B alloy with lattice parameter  $a_0$ .

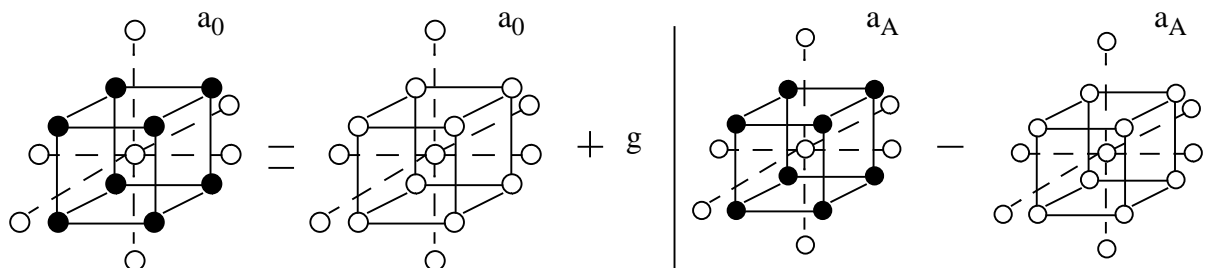


Fig.9: Schematic representation of the contribution of an A atom (center of the cube) to the energy of formation of B2 A-B compound with lattice parameter  $a_0$ . The left hand side represents the actual B2 structure. The first term in the left hand side indicates the strain energy environment (all atoms are of type A, in the lattice of the alloy) and the second and third term (between brackets) indicate the chemical energy environment and the reference chemical energy environment, respectively.

would also derive the corresponding coupling functions  $g_A$  and  $g_B$ , according to Eq. 15.

Fig. 10 shows the environment assumed in the calculation of the chemical energy. Since in the example given, both pure crystals are of the same crystallographic structure as the alloy, the calculation is particularly simple, and it only requires noticing that the lattice parameter for each case is the equilibrium lattice parameter of the pure crystals ( $a_A$  and  $a_B$ ).

The BFS equation for the calculation of the chemical energy contribution for atom A is

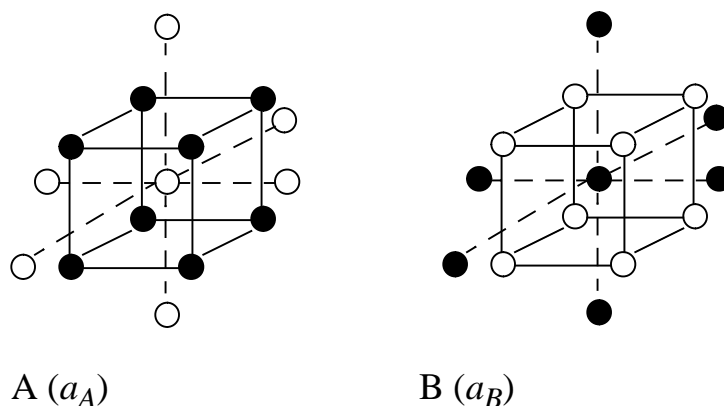


Fig. 10: Environment seen by atoms A and B, respectively, for the calculation of the BFS chemical energy contribution. Note that the actual atomic composition of the alloy is preserved, but the lattice parameters used for each case corresponds to that of the equilibrium pure crystals A and B, respectively.



$$8R_1^{p_A} e^{-\alpha_A R_1} + 6R_2^{p_A} e^{-\left(\alpha_A + \frac{1}{\lambda_A}\right)R_2} = 8r_A^{p_A} e^{-(\alpha_A + \Delta_{BA})r_A} + 6a_A^{p_A} e^{-\left(\alpha_A + \frac{1}{\lambda_A}\right)a_A} \quad (20)$$

where  $r_A$  is the equilibrium nearest neighbor distance in a crystal A. Note that atom A interacts with 8 nearest neighbors of species B (thus the factor  $\alpha_A + \Delta_{BA}$  in the first term of the r.h.s. of Eq. 20) and that all 6 of its next-nearest neighbors are of the same atomic species A. This equation is solved for the equivalent lattice parameter  $a_C$  and the chemical energy contribution is

$$e_C^A = \gamma_A E_C^A \left( 1 - (1 + a_C^{A*}) e^{-a_C^{A*}} \right) \quad (21)$$

where the scaled lattice parameter of the (chemical) equivalent crystal is given by

$$a_C^{A*} = q \frac{(a_C^A - a_A)}{l_A} \quad (22)$$

and where  $\gamma_A = 1$  or  $-1$ , depending on whether the scaled lattice parameter is positive or negative. A similar calculation is performed for atom B, replacing the appropriate parameters. In particular, note that the interaction parameter in the exponential in the first term of the r.h.s. of Eq. 20 is now  $\alpha_B + \Delta_{AB}$ , as all the nearest neighbors of the reference B atom are of species A (Fig. 10).

In this particularly simple example, it is not necessary to compute the reference chemical energy ( $e_{C_0}$ ) for either type of atom, as the corresponding environments correspond to perfect equilibrium A and B crystals already. Therefore, the total chemical energy contributions are

$$\epsilon_C^A = e_C^A \text{ and } \epsilon_C^B = e_C^B.$$

We finally write the following expression for the energy of formation  $\Delta H$  of the B2 structure A-B:

$$\Delta H = \frac{1}{2}(e_S^A + g_A \epsilon_C^A + e_S^B + g_B \epsilon_C^B) \quad (23)$$

While this expression applies to this stoichiometric binary system characterized by one atom of each atomic species, in more complex situations the calculation might involve considering more non-equivalent atoms. In this example the Ni atoms locate themselves in one simple cubic sublattice and the Al atoms in the other. As such, all Ni or Al atoms are respectively identical and contribute the same amount to the energy of formation. Therefore, the BFS calculations have to be performed for just one atom of each species. The simplicity of this calculation allows for a straightforward determination of the BFS parameters in terms of the energy of formation and equilibrium lattice parameter of the binary base alloy (NiAl). In the following subsection, we will refer to the scheme used in this work for parameterizing the binary system at hand.

### *Parameterization of the BFS Method*

The previous example indicates that beyond the approximate scheme developed to simulate the process of alloy formation (i.e. separating strain and chemical contributions), the power and accuracy of the method are heavily dependent on the parameters used both for the individual elements ( $p$ ,  $l$ ,  $a_e$ ,  $E_c$ ,  $\lambda$ ) and those used for each type of binary combination that might appear in the system ( $\Delta_{AB}$  and  $\Delta_{BA}$ ). Also, this example highlights the extreme simplicity of the method when the crystallographic structure of the alloy is the same as that of the constituents (in the example,

both A and B were bcc elements and the alloy formed is also bcc-based). While in general it is not known what is the phase structure of an alloy for a certain composition, some basic knowledge can be used *a priori* to simplify the calculations.

Take, for example, the system to be studied in this work:  $\beta$ -NiAl. This binary alloy is known to have the B2 structure, in spite of the fact that each of its constituents are fcc elements. Assuming the existence of a bcc phase of Ni as well as for Al would reduce the complexity of the calculation to a level similar to the example just discussed. If the BFS method relied only on experimental input for the determination of the necessary parameters listed above, it would make this approach impossible to implement under most circumstances. However, first-principles methods can be used in a straightforward manner to determine the physical properties of these elements (bcc-Ni and bcc-Al) even if they do not exist naturally. In doing so, not only do we eliminate the dependence of the BFS method on sometimes uncertain or non-existent experimental input, but we also generate a consistent approach. This approach simplifies the numerical complexity of the problem and also introduces a systematic procedure for the generation of the necessary parameterization, since they would all be computed by the same method, with the same level of approximation.

To determine these parameters, we used the Linear-Muffin-Tin-Orbital (LMTO) [27] method in the Atomic Sphere Approximation (ASA). This scheme was used to calculate the equilibrium properties (cohesive energy  $E_c$ , equilibrium lattice parameter  $a_e$ , and bulk modulus  $B_0$ ) of the elemental solids in the same crystal symmetry as that of the compound to be studied (bcc). This set of parameters is accurately described by the Local Density Approximation [28]. In this work, we generated parameters for Ni, Al, Ti, Cr and Cu in the bcc symmetry, as well as the B2 structures of each of the pairs formed (only B2 NiAl and NiTi exist in nature) for the determination of the

BFS parameters  $\Delta_{AB}$  and  $\Delta_{BA}$ . The parameters for Ti, Cr and Cu will be used and validated in subsequent papers in this series.

The LMTO method uses a minimal basis set. For this work, we only used  $s$ ,  $p$  and  $d$  orbitals. All calculations were done with equivalent sampling of the Brillouin zone using, for the bcc lattice, 120  $k$ -points in the irreducible wedge. The basis set and sampling of the Brillouin zone used for the calculation of the B2 compounds was equivalent to that used for the pure elements. We refer the reader to Refs. 27-28 for a detailed discussion of the LMTO method. The pure element LMTO-generated parameters  $p$ ,  $l$ ,  $E_c$ ,  $a_e$  and the resulting value of  $\alpha$  are displayed in Table 1 for Ni and Al.

The simplicity of the BFS formalism allows for a straightforward method for determining the BFS parameters  $\Delta_{AB}$  and  $\Delta_{BA}$  by an analytical procedure that not only eliminates numerical errors but also sheds light on the range of validity of the resulting parameters. Leaving the details of the determination of the BFS parameters to Appendix 1, we list in Table 2 the resulting values for  $\Delta_{NiAl}$  and  $\Delta_{AlNi}$ .

### *Other theoretical methods applied to intermetallics*

As mentioned in the Introduction, there has been substantial progress in the last two decades in the area of theoretical techniques and their relevance in dealing with systems of practical importance. Current techniques range from those that impose an empirical parameterization of the constants in Ising Hamiltonians [29-33] or those that parameterize experimental databases [34], families of semiempirical methods based on the determination of interatomic potentials [11-15], to all-electron first principles calculations [35-44]. Recent first-principles calculations include the

full-potential linearized augmented Slater-type orbital method (LASTO) used by Alatalo et al., in their analysis of the complex Zr-Al phase diagram [40], the first-principles discrete variational method study of disordered Fe-V alloys by Krause et al. [41], a detailed study of composition and phase diagrams of Cu-Au, Ag-Au, Cu-Ag and Ni-Au by Ozolins et al. [42], and the determination of formation energies for Fe<sub>3</sub>Al by Mayer et al. [43]. These, and other similar studies, concentrate mostly on monatomic [12,44] or binary systems.

In terms of semiempirical techniques, current work on NiAl alloys include the extensive analysis of this system by Farkas et al., in a series of recent articles where the embedded atom method is modified for its use in this system [45-46]. Other techniques currently used include Finnis-Sinclair potentials specifically determined for NiAl [47], tight-binding methods [12,44] (still mostly restricted to single element systems), and potentials determined from first-principles calculations. This last group includes the work of Zhang et al. in Fe-Al and Ni-Al alloys [48], and the study of transition metal aluminides by Moriarty and Widom [49].

Other relevant work in this area includes the extension of Miedema's semiempirical model for point defects in B2 compounds by Bakker et al. [34] and the development of semiempirical N-body non-central potentials for FeAl alloys by Besson and Morillo [50].

In terms of ternary NiAl+X systems, very little progress has been made relative to that made for binary alloys, although it is expected that the development of accurate potentials and efficient computational methods, will generate growth in this area in the near future. Most notably, recent theoretical work of the influence of ternary additions to NiAl includes the Monte Carlo analysis of NiAl+Ti alloys by Sumin et al. [51], and the statistical theory of ordering combined with the electronic theory of alloys in the pseudopotential approximation by Mekhrasov et al. [52].

As we increase the complexity of the system at hand, as will clearly be the case in the subse-

quent papers in this series, we will have little if any previous theoretical work for comparison. Once we move beyond ternary systems, all our results will become purely of a predictive nature, relying on experimental verification.

## RESULTS AND DISCUSSION

The BFS calculations for B2 NiAl were performed on a 72-atom cell, allowing for atomic relaxation induced by the presence of vacancies and substitutional atoms. However, relaxations were allowed only at a global level in the sense that the lattice parameter of the cell as a whole was varied until the energy was minimized. A more detailed study, which we consider unnecessary for the goals of this work, would include the possibility of local atomic relaxations in the vicinity of defects. This issue, and its consequences on the phase structure, will be dealt with in forthcoming papers.

In a cell of this size there is a large number of possible distributions of Ni and Al atoms for any given alloy composition. Knowing the behavior of each and every one of them would be unnecessary (in this case, considering *all* the possible distributions of Ni and Al atoms as well as vacancies, in a 72-site cell), as most of the information needed for determining the defect structure can be obtained from a few selected situations where the essential defect structures are considered. Therefore, instead of searching for an absolute energy minimum for a given number of Ni and Al atoms located in every available lattice site with any specific short and long order scheme, we chose to construct a selected, but sufficiently large number of 'candidate' distributions to obtain information on the energetics of the system close to the ground state. These configurations are still, to a certain extent, arbitrary, and may not necessarily include the ground state for a given

composition. However, it is clear that when creating a catalogue of selected configurations which consider the most likely atomic distributions, one would obtain not only the necessary information (i.e., the lowest energy state for each concentration) but also additional information on general trends in defect structures. While most of the configurations included in the catalogue are experimentally inaccessible, they serve the purpose of determining trends in the bulk properties of the actual alloys. Moreover, if the set of configurations sampled is sufficiently large and the structures are properly chosen, respecting the symmetries that characterize the system, one would expect to find the ground state or states sufficiently close to it at each composition.

As a consequence, an additional advantage of this approach is that it enables us to determine an ‘energy spectrum’, showing how alternative ordering schemes compare energetically with the lowest energy state for each composition. The magnitude of the energy gaps between alternative distributions and the ground state should be proportional to the probability of finding these configurations in the actual alloy. Figure 11 includes representative samples of the catalogue of configurations used in this work, first showing the basic 72-atom cell (Fig. 11.a) followed by a few cases that include substitutional defects, antistructure atoms and vacancies (Fig. 11.b-d).

Based on stoichiometric NiAl, Appendix 2 introduces a simple way of characterizing each one of the configurations included in the catalogue of structures we examined. Due to the large number of configurations included, only a small but representative number of them are graphically shown in Fig. 11. The rest are described in a notational shorthand discussed in Appendix 2.

The analytical procedure is then straightforward. The BFS method is applied to each one of the configurations included in the catalogue in order to determine its energy of formation as well as the equilibrium lattice parameter (for which the total energy of formation is minimized). Appendix 2 also includes these BFS results for each configuration.

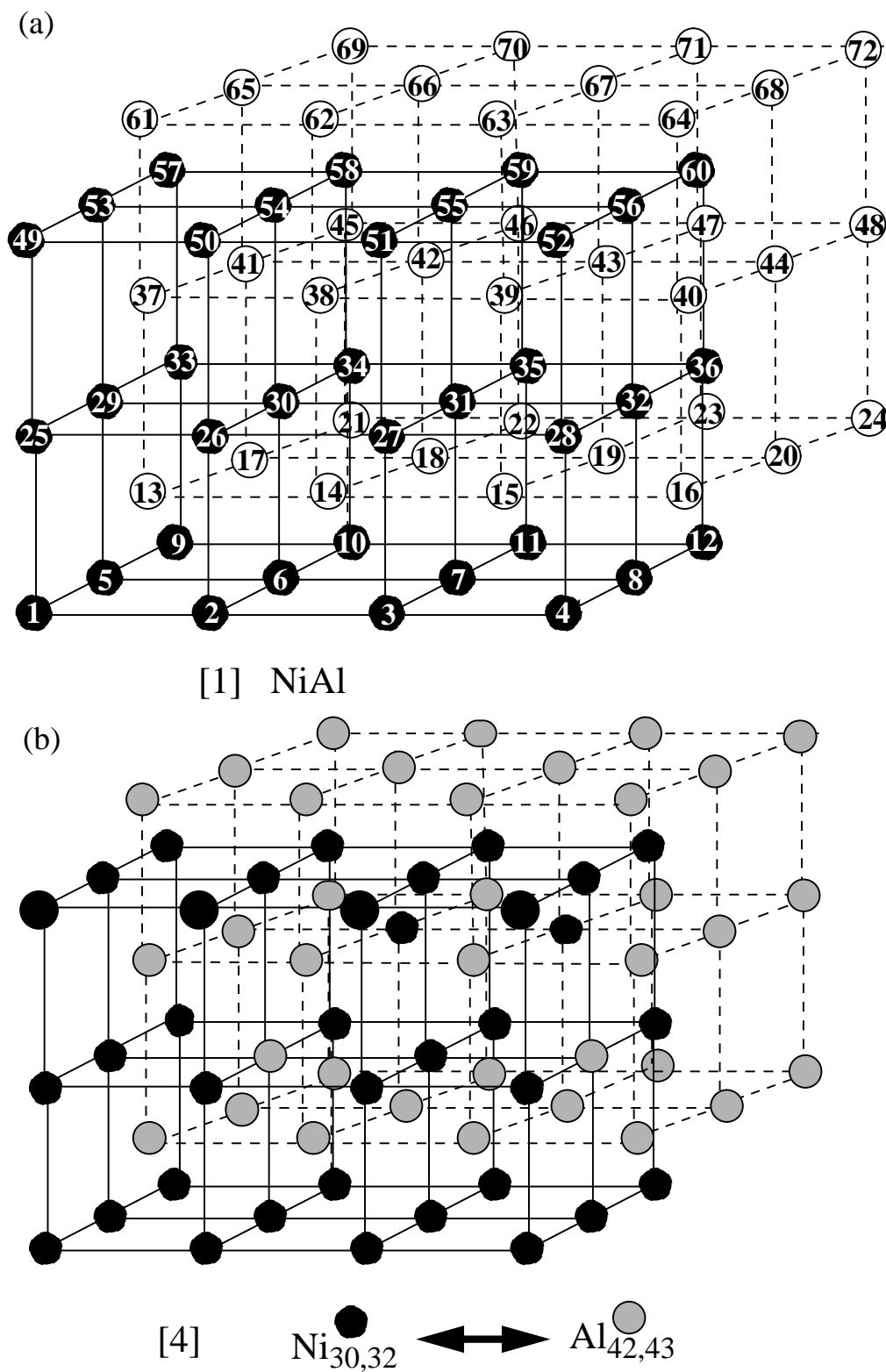
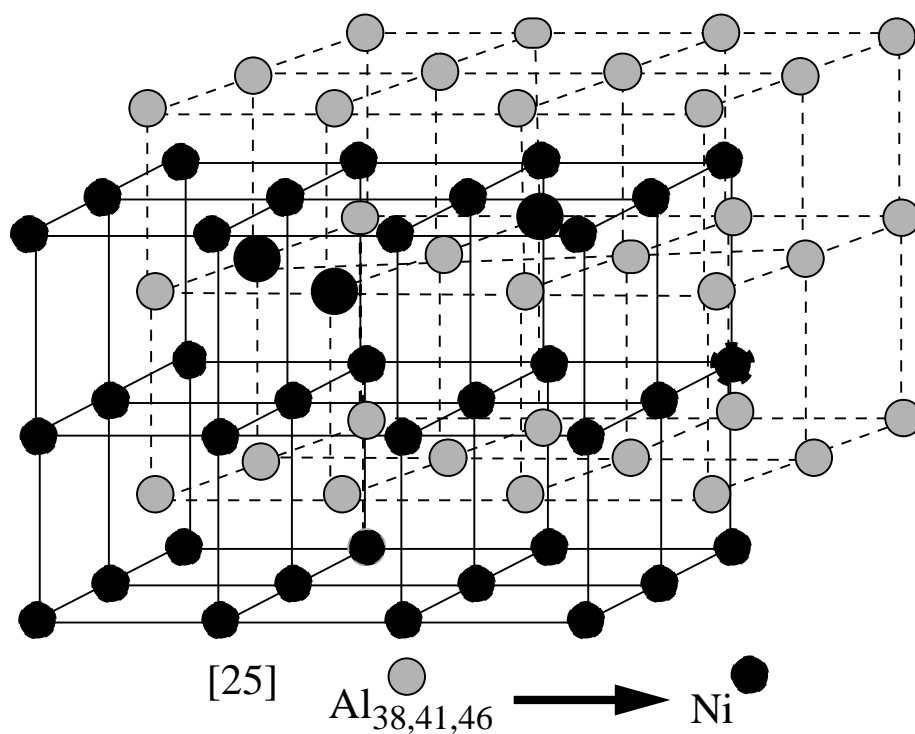


Fig. 11: (a) The computational cell used to generate the catalogue shown in Appendix 2. (b) Sample of a NiAl cell showing two site exchanges (see [4] in the catalogue).



(c)



(d)

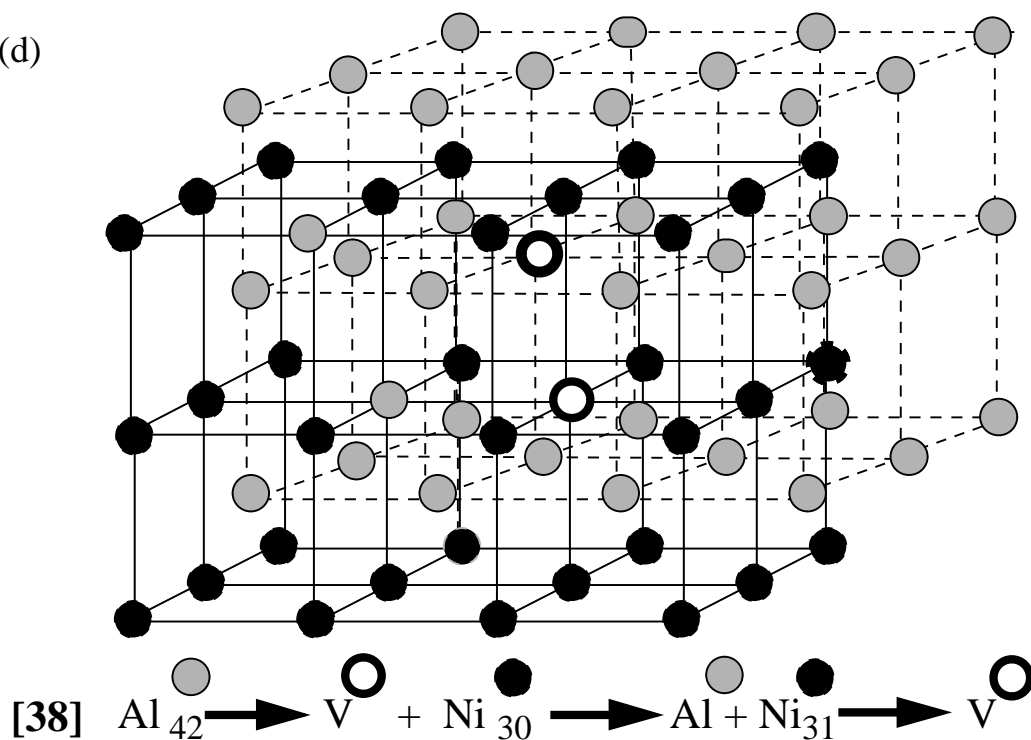


Fig. 11 (continued): (c) Sample of a  $\text{Ni}_{52.78}\text{Al}_{47.12}$  alloy where Al atoms at lattice sites 38, 41 and 46 are replaced by Ni atoms (see [25] in the catalogue in Appendix 2). (d) Sample of a  $\text{Ni}_{47.83}\text{Al}_{52.17}$  alloy, where the Al atom at lattice site 42 is replaced by a vacancy, the Ni atom at lattice site 30 is replaced by an Al atom, and the Ni atom at lattice site 31 is replaced by a vacancy (see [38] in the catalogue).

Fig. 12 displays some of the results for representative configurations in the catalogue. The results are shown in the form of an energy spectrum, which shows a clear comparison of the energetics of the various atomic arrangements. Each column in this spectrum corresponds to specific compositions of  $\text{Ni}_{50+x}\text{Al}_{50-x}$  alloys, denoted by the Ni atomic concentration. Each energy level is identified by the catalogue number used in Appendix 2. The lowest energy configuration (lowest level in the first column in Fig. 12) corresponds to the perfect B2 structure, where all Ni and all Al atoms populate their own interpenetrating sublattices. Higher energy configurations represent a wide variety of defects. Moving up in the spectrum, we first find a group of levels very close in energy which correspond to the presence of antistructure atoms, where a pair of Ni and Al atoms switch places. The small differences in energy between these levels relates to the relative position of the two antistructure atoms (being smallest when they are nearest-neighbors). After another comparable gap in energy, we found states with two antistructure pairs and so on. Similar situations are found at higher Ni concentrations. The lowest energy configuration for a given concentration in Ni-rich alloys always corresponds to a pure substitutional state and higher energy states include additional swaps of atoms between Ni and Al sites. For the highest Ni concentration shown (55.55 at. % Ni), the purely substitutional case distinguishes between the configuration where the substitutional atoms are as far away from each other as possible, to configurations with slightly higher energy where the substitutional atoms display a clustering tendency.

This spectrum emphasizes both the completeness of the catalogue selected (i.e. the lowest energy state is properly identified for every concentration) as well as its shortcomings: some high energy states (2 for 50 at. % Ni; 19 for 51.39 at. % Ni), characterized by clustering of antistructure atoms) are missing at higher concentrations. On the other hand, the high energy state 27 for 55.55 at. % Ni is comparable to 8 for 50 at. % Ni, both including specific alignment of the antistructure

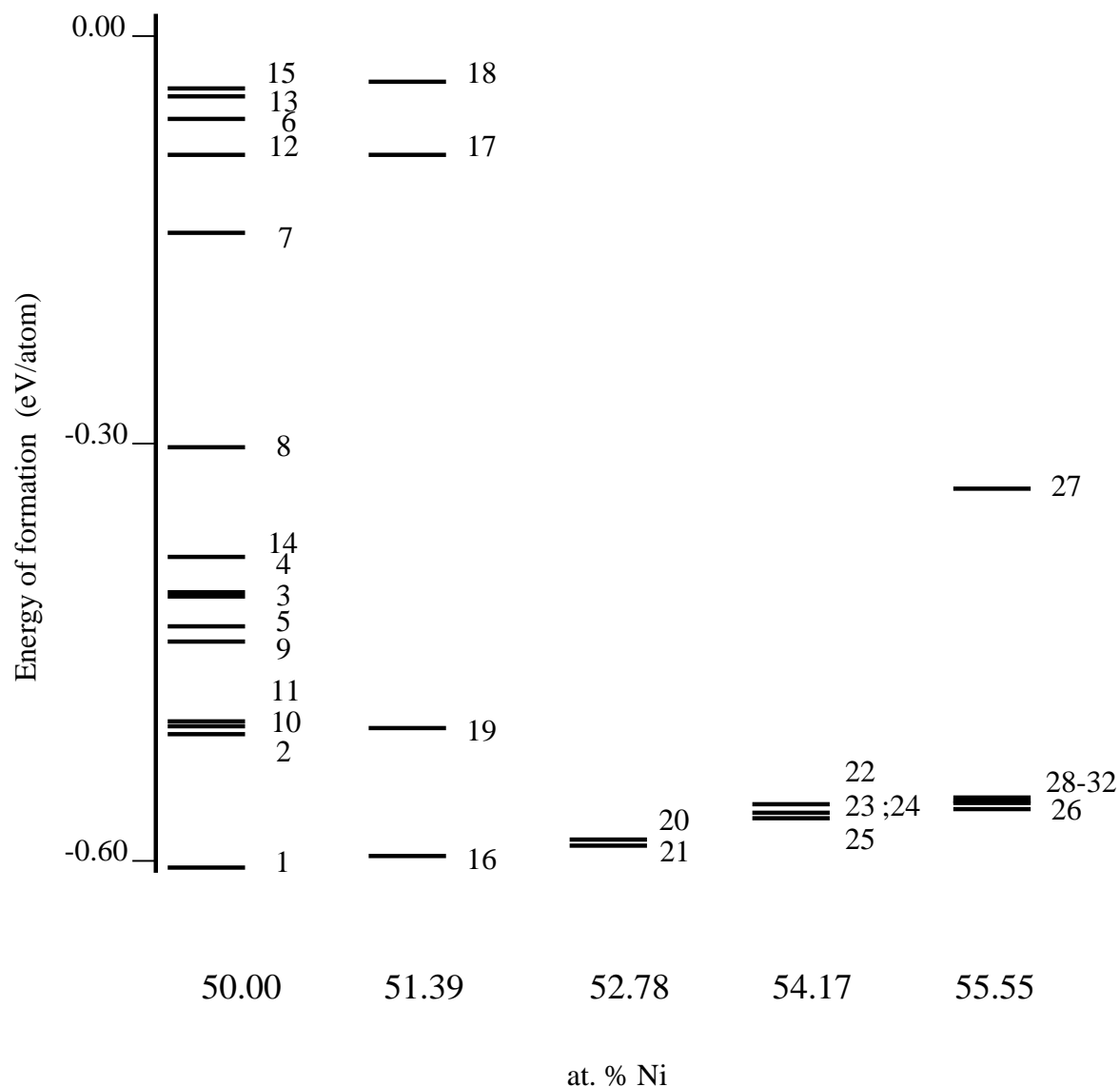


Fig. 12: ‘Energy spectrum’ for substitutional defect structures in Ni-rich NiAl alloys. Each column represents a specific binary alloy concentration. The levels represent the energy of formation of configurations specified in the catalogue (the numbers by each level identify the configuration in Appendix 2). All the configurations included in this Figure correspond to substitutional alloys exclusively (no vacant sites). In all cases, the lowest energy configuration corresponds to Ni atoms occupying available Al sites. Higher energy states include various antistructure defects.

atoms in specific planes and directions (see Appendix 2). The smaller energy gap between this type of configuration and the lowest energy state for higher Ni concentrations hints at the possibility that this type of defect might occur in the actual alloy.

Fig. 13 shows similar results for Al-rich alloys, indicating not only that the lowest energy states arise from the presence of Ni vacancies but also that selected antistructure-vacancy combinations could also be present. Experimental evidence confirms these results [4-9].

The determination of the lattice parameter for each configuration is done by minimizing the energy of the cell with respect to the lattice spacing of the cell as a whole but not allowing for individual anisotropic relaxations. While performing detailed calculations including individual atomic relaxations is well within the computational efficiency of the method, such lengthy calculations would become impractical for higher order alloys. We therefore compromise between accuracy and simplicity assuming that whole-cell isotropic relaxations will be sufficient for describing the energetics of these alloys.

The wealth of information embedded in Fig. 12 can be used to gain further insight in the dependence of the lattice parameter  $a(x)$  of  $\text{Ni}_{50+x}\text{Al}_{50-x}$  alloys. While it is natural to determine  $a(x)$  from the values of  $a$  corresponding to the lowest energy states for each concentration, as depicted in Fig. 12, it is interesting to first visualize the lattice parameter of alternative, higher energy, structures by choosing characteristic values for each ‘band’ (group of energy levels close in energy) in Fig. 12.

Fig. 14 displays the lattice parameter as a function of Ni concentration for a portion of the set of ‘candidate’ configurations, regardless of the energy of the configuration. Each point corresponds to a distinct arrangement of Ni and Al atoms as well as vacant Ni or Al sites in the calculational cell. We focus our attention on three particular regimes that can be seen in Fig. 14: an

inverted V-shaped set of filled symbols with its apex at the stoichiometric composition, a line of circles indicating structures with increasing lattice parameter with increasing Al content, and a large number of configurations enclosed by the boundary line consisting of filled symbols. The configurations denoted by filled symbols represent the lowest energy configurations at each composition. The ascending line of circles corresponds to configurations where no vacancies are present and increasing numbers of Al atoms occupy Ni sites, a typical substitutional defect struc-

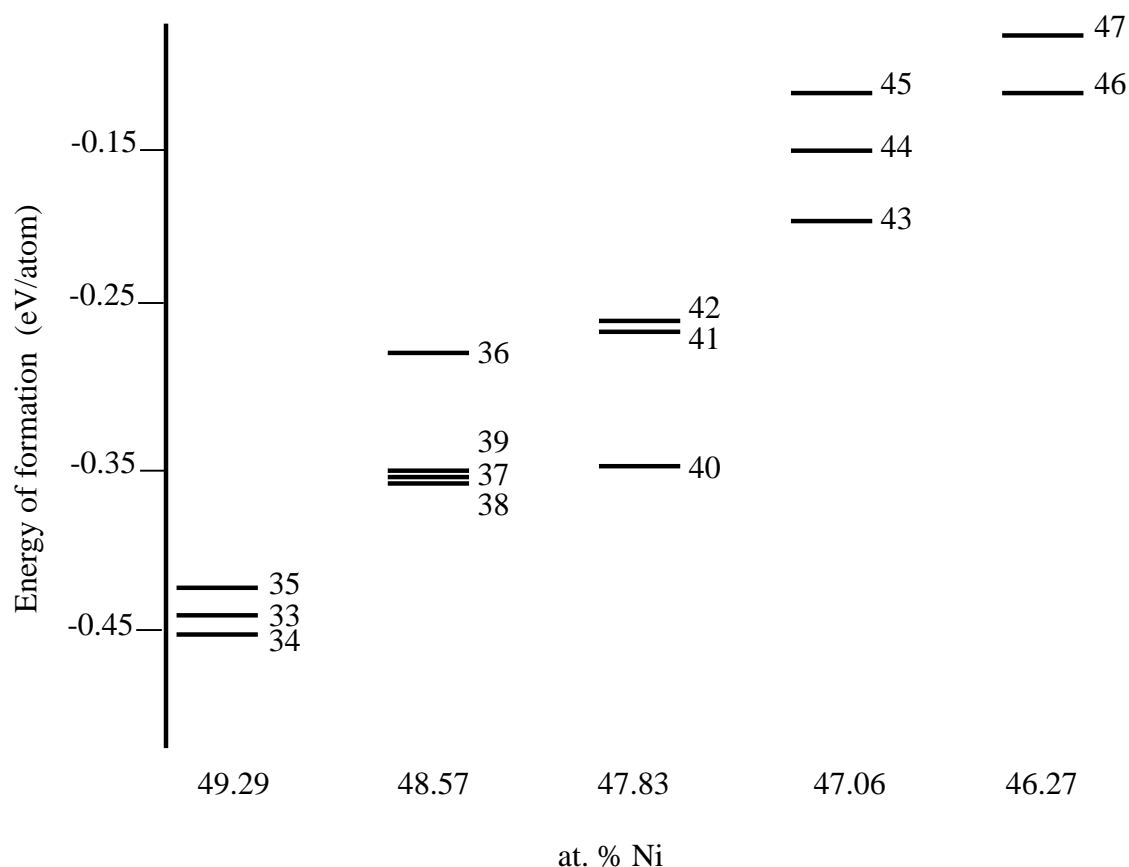


Fig. 13 : Energy spectrum for Al-rich NiAl alloys containing vacancies. For  $x_{\text{Ni}} = 49.29$ , the lowest energy state corresponds to an Al atom in a Ni site and a nearest-neighbor vacant Al site (34), a vacant Ni site (33) and an Al atom in a Ni site and a distant vacant Al site (35), in order of increasing energy. For  $x_{\text{Ni}} = 48.57$ , the lowest (two-vacancy) state corresponds to an Al anti-structure atom and a nearest-neighbor pair of vacancies in Ni and Al sites (38) with almost the same energy of formation as a configuration with two vacant Ni sites (37). For higher Al concentrations, the lowest energy state is always one with vacant Ni sites (40, 43, 46).

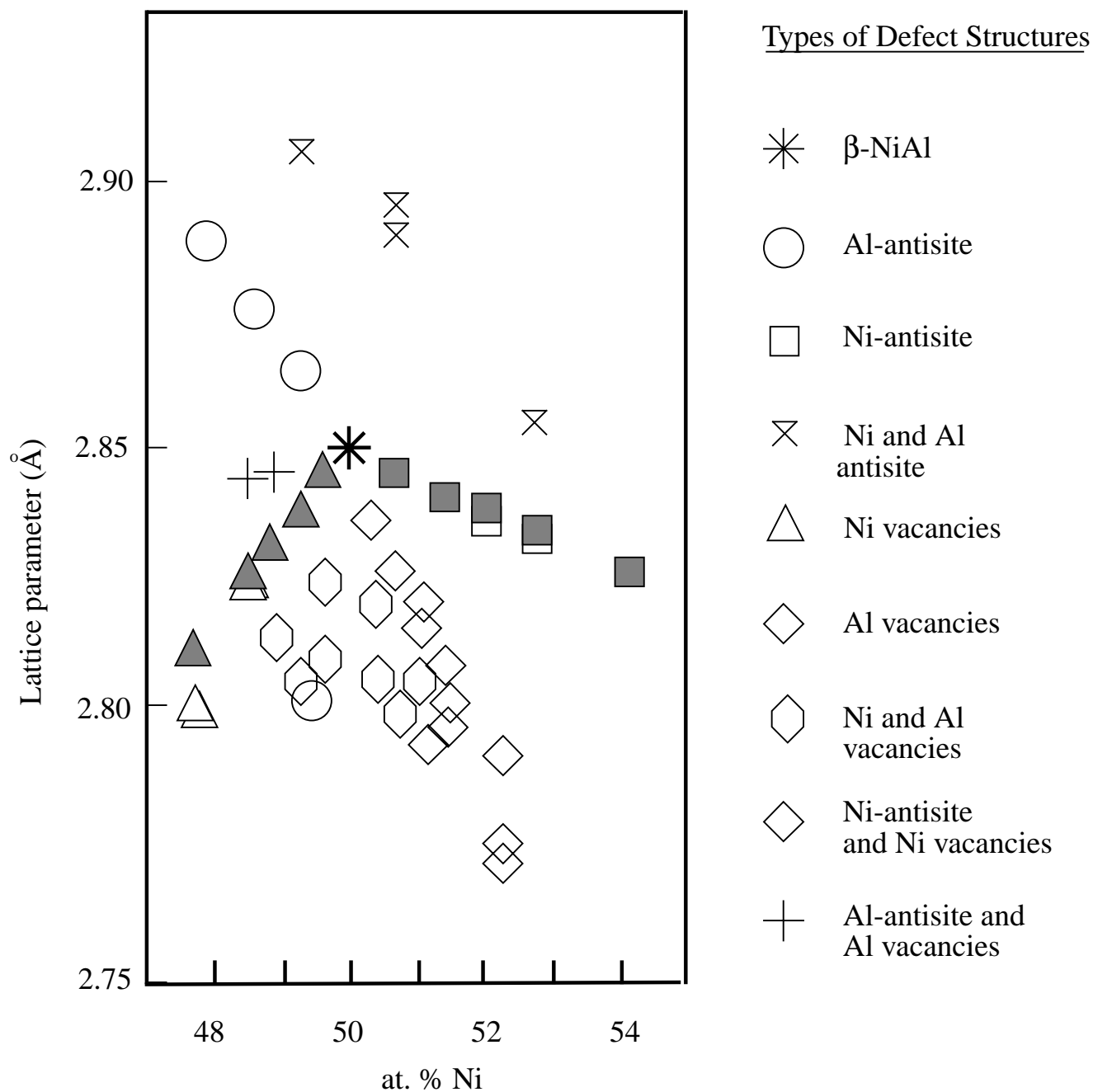


Fig. 14: Lattice parameter (in Å) as a function of Ni concentration for various candidate defect structures. Different symbols indicate alloys with different types of general defect structures. Similar symbols for the same composition correspond to different distributions of the same defect within the computational cell. The shaded symbols correspond to those configurations with the lowest energy for that composition.

ture. While substitutional states have the lowest energy for each concentration in the Ni-rich side, the opposite is true for the 45-50 at. % Ni concentration range. The cluster of points enclosed by the inverted V-shaped boundary correspond to configurations characterized by random distributions of vacancies in Al or Ni sites as well as random exchanges of Ni and Al atoms from their equilibrium stoichiometric locations. Stoichiometric  $\beta$ -NiAl is noted by an asterisk.

A comparison of the modeled results with experimental data for the lattice parameter of various NiAl alloys is displayed in Fig. 15. The theoretical results, shown as a continuous line, consist of the calculated lattice parameter and density for the lowest energy configuration observed at each composition. The lattice parameter results from the lowest energy configurations on the Ni-rich side of stoichiometry, show excellent agreement with experimental data (Fig. 14). The linear regime in the density (Fig. 15.a) and lattice parameter (Fig. 15.b) vs. Ni concentration for the range 50-60 at.% Ni is almost exactly reproduced by our calculations. A recent review paper by Noebe et al. [53] provides a convenient linear description of the available experimental results, both for the lattice parameter  $a$  and density  $\rho$  vs. Ni concentration. To highlight the agreement between theory and experiment, we therefore compare those expressions with ones corresponding to the BFS results. For comparison purposes, both quantities were normalized to the stoichiometric NiAl values ( $a_0$  and  $\rho_0$ , for the lattice parameter and density, respectively), as there is a slight difference of 1.2 % between the experimental ( $a_0 = 2.887 \text{ \AA}$ ) and LMTO values ( $a_{Theor} = 2.85 \text{ \AA}$ ) for the lattice parameter of the stoichiometric B2 NiAl structure. The expressions for experimental and theoretical results on the Ni-rich side of stoichiometry are

$$\left(\frac{\rho}{\rho_0}\right)_{Exp} = 0.5339 + 0.009322x_{Ni} \quad (24)$$

and

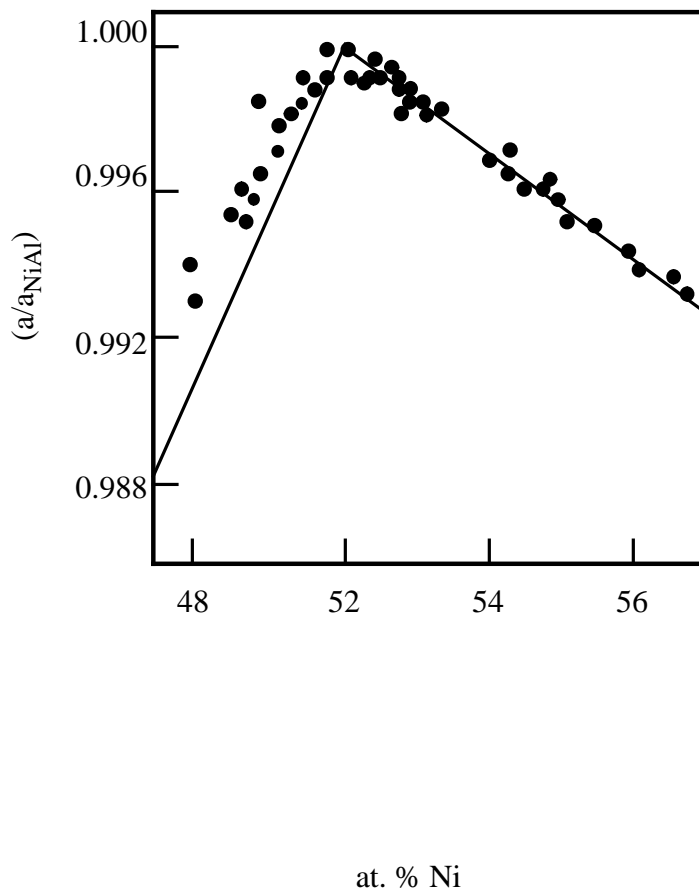
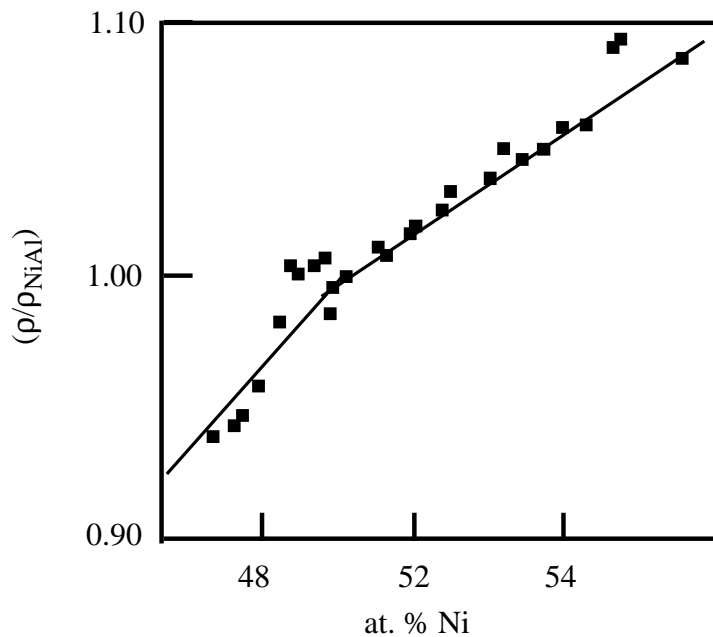


Fig. 15 : (a) Density and (b) lattice parameter of binary alloys as a function of Ni concentration, normalized to their stoichiometric values. The solid symbols denote experimental results from different investigators (see Ref. 53). The lines denote the BFS predicted properties (see text), corresponding to the structure with the lowest energy state for each composition.



$$\left(\frac{\rho}{\rho_0}\right)_{Theor} = 0.5324 + 0.009352x_{Ni} \quad (25)$$

for the density (relative to the stoichiometric NiAl density) and

$$\left(\frac{a}{a_0}\right)_{Exp} = 1.0384 - 0.0007914x_{Ni} \quad (26)$$

and

$$\left(\frac{a}{a_0}\right)_{Theor} = 1.0396 - 0.0007689x_{Ni} \quad (27)$$

for the lattice parameter (relative to the stoichiometric NiAl value) for Ni concentrations,  $x_{Ni}$ , between 50 and 60 at. % .

On the Al-rich side of stoichiometry a more complicated defect structure is observed. The lowest energy states on the Al-rich side correspond to arrangements of vacancies with no change in site occupancy for the Ni and Al atoms with respect to their original sublattice in NiAl. In the lowest energy configurations, the Ni vacant sites are at next-nearest neighbor distance from each other. In other words, clustering of the defects results in the lowest energies. Once again, the ensuing values for the lattice parameter and the density as a function of Ni concentration (closed triangles in Fig. 14) can be described by linear relationships and compared to the experimental values [19]:

$$\left(\frac{\rho}{\rho_0}\right)_{Exp} = 0.02x_{Ni} \quad (28)$$

and

$$\left(\frac{\rho}{\rho_0}\right)_{Theor} = 0.19914 + 0.01602x_{Ni} \quad (29)$$

for the density (relative to the stoichiometric NiAl value) and

$$\left(\frac{a}{a_0}\right)_{Exp} = 0.924148 + 0.001517x_{Ni} \quad (30)$$

and

$$\left(\frac{a}{a_0}\right)_{Theor} = 0.840261 + 0.003184x_{Ni} \quad (31)$$

for the lattice parameter (relative to the stoichiometric NiAl equilibrium value) for  $x_{Ni}$  between 45 and 50 at. %.

While not directly apparent from Fig. 14, this work also showed that locally ordered arrangements of defects were energetically preferred to random distributions of point defects. For example, in Fig. 14 at 47.82 at. % Ni there are an open and filled triangle of very similar lattice parameter. The difference in these points is that the input structure of the lowest energy configuration (solid triangle) was composed of a greater degree of ordering of Ni-vacancies. While overall structures composed of Ni-vacancies had the lowest energy at a given composition, a similar trend of lower energy with increasing ordering of point defects was observed within the other types of defect arrangements as well. For example, within the family of configurations composed of Al-vacancies plus Ni-vacancies, the configurations (hexagons) with lattice parameters closest to those of the ground state consisted of locally ordered arrangements of vacancies (i.e. an Al vacancy shared by two Ni-vacancies at the nearest neighbor distance) while those configurations with higher energy consisted of more random distributions of point defects.

This also hints at the possibility that the actual defect arrangements on the Al-rich side of stoichiometry may be more complicated than normally assumed. A complete treatment of tempera-

ture and local relaxation effects would be necessary to absolutely rule out the existence of these more complicated structures consisting of ordered arrangements of Ni and Al vacancies in Al-rich alloys. But even that would not rule out the possibility that these structures may actually be observed as metastable states since their energy is not that different from defect structures composed solely of Ni-vacancies.

## CONCLUSIONS

We introduced a formalism that combines the type of results achieved by first-principles methods with the convenience of semiempirical methods for a simple and straightforward analysis of situations that cannot be treated in a similar fashion by either individual technique. An intuitive as well as a formal description of the BFS method was presented, with the goal of familiarizing the reader with the concepts to be used in this and subsequent papers in this series on NiAl-based alloy design. Beyond the operational equations, we introduced other elements that will be heavily used when dealing with higher order alloys. These include the definition of a catalogue of predetermined configurations (as opposed to lengthy computational algorithms for the search of minimum energy structures), the use of energy spectra to identify trends and to gain insight on metastable structures (as opposed to just dealing with lowest-energy states), and the description of the observed behavior in terms of BFS strain and chemical energies.

As our first test of the BFS method we analyzed the defect structure of binary NiAl alloys. Our theoretical modeling of the defect structure of  $\beta$ -NiAl alloys is fully consistent with the conclusions drawn from experimental evidence indicating that substitutional defects dominate in Ni-rich alloys and that the presence of vacancies is responsible for the sharp decrease in lattice

parameter with increasing Al content in Al-rich alloys. Moreover, the results hint to the possibility that a more complex defect structure exists: the presence of vacancies both in the Ni and Al sublattice in Al-rich alloys and a preference for clustering or local ordering instead of a random distribution of point defects with any deviation in stoichiometry. In future papers we will build on these results by modeling ternary and higher order alloys.

## REFERENCES

1. Bozzolo, G. and Ferrante, J., J. Computer-Aided Mater. Design 2 (1995) 113, and references therein.
2. Darolia, R., in Structural Intermetallics, ed. by R. Darolia et al., The Minerals, Metals and Materials Society, Warrendale, PA, 1993, pp. 495.
3. Noebe, R. D. and Waltson, W. S., in Structural Intermetallics 1997, ed. by M. V. Nathal et al., The Minerals, Metals and Materials Society, Warrendale, PA, 1997, pp. 573.
4. Bradley, A. J. and Taylor, A., Proc. R. Soc. A 159 (1939) 232.
5. Taylor, A. and Doyle, N. J., J. Appl. Cryst. 5 (1972) 201.
6. Georgopolous, P. and Cohen, J. B., Scripta Metall. 11 (1977) 147; *ibid.*, Acta Metall. 29 (1981) 1535.
7. Guseva, L. N., Doklady. Akad. Nauk. 77 (1951) 415.
8. Cooper, M. J., Philos. Mag. 8 (1963) 805.
9. Kogachi, M., Minamigawa, S. and Nakahigashi, K., Acta Metall. 40 (1992) 1113.
10. Faulkner, J. S., Moghadam, N. Y., Wang, Y. and Stocks, G. M., Phys. Rev. B 57 (1998) 7653.
11. Baskes, M. I., Materials Chemistry and Physics 50 (1997) 152.

12. Yang, S. H., Mehl, M. J. and Papaconstantopolous, D. A., Phys. Rev. B 57 (1998) R2013.
13. Norskov, J. K. , Phys. Rev. B 20 (1979) 446.
14. Foiles, S. M. and Daw, M. S., J. Mater. Res. 2 (1987) 5.
15. Wallace, W. E. and Ackland, G. J., Surf. Sci. Lett. 275 (1992) L685.
16. Good, B., Bozzolo, G. and Ferrante, J., Phys. Rev. B 48 (1993) 18284.
17. Bozzolo, G., Amador, C., Ferrante, J. and Noebe, R. D., Scripta Metall. 33 (1995) 1907.
18. Bozzolo, G., Ferrante, J. and Smith, J. R., Phys. Rev. B 45 (1992) 493.
19. Bozzolo, G. and Ferrante, J., Phys. Rev. B 45 (1992) 12191; Bozzolo, G., and Ferrante, J., Scripta Metall. 26 (1992) 127.
20. Bozzolo, G., Ibanez-Meier, R. and Ferrante, J., Phys. Rev. B 51 (1995) 7207.
21. Bozzolo, G. and Ferrante, J., Ultramicroscopy 42/44 (1992) 55.
22. Bozzolo, G. Noebe, R. D., Garg, A., Ferrante, J. and Amador, C., Mat. Res. Soc. Symp. Proc. 460 (1997) 443.
23. Kobistek, R., Bozzolo, G., Ferrante, J. and Schlosser, H., Surf. Sci. 307-309 (1994) 390.
24. Smith, J. R., Perry, T., Banerjee, A., Ferrante, J. and Bozzolo, G., Phys. Rev. B 44 (1991) 6444.
25. Bozzolo, G., Ferrante, J. and Rodriguez, A. M., J. Computer-Aided Mater. Design 1 (1993) 285.
26. Rose, J. H., Smith, J. R. and Ferrante, J., Phys. Rev. B 28 (1983) 1835; Rose, J. H., Smith, J. R., Guinea, F. and Ferrante, J., Phys. Rev. B 29 (1984) 2963.
27. Andersen, O. K., Postnikov, A. V. and Savrasov, S. Y., Mat. Res. Soc. Symp. Proc. 253 (1992) 37.

28. Hohenberg, P., and Kohn, W., Phys. Rev. 136 (1964) B864; Kohn, W. and Sham, L. J., Phys. Rev. 140 (1965) A1133.
29. Shockley, W. , J. Chem. Phys. 6 (1938) 130.
30. Cowley, J. M., Phys. Rev. 77 (1950) 669.
31. van Baal, C. M., Physica (Amsterdam) 64 (1973) 571.
32. Golosov, N. S., Popov, L. E. and Pudan, L. Y., J. Phys. Chem. Solids 34 (1973) 1149.
33. Kikuchi, R., J. Chem. Phys. 60 (1974) 1071.
34. Bakker, H., Modder, I. W., and Kuin, M. J., Intermetallics 5 (1997) 535, and references therein.
35. Terakura, K., Oguchi, T., Mohri, T. and Watanabe, K., Phys. Rev. B 35 (1987) 2169.
36. Sanchez, J. M., Stark, J. P. and Moruzzi, V. L., Phys. Rev. B 44 (1991) 5411.
37. Amador, C. and Bozzolo, G., Phys. Rev. B 49 (1994) 956.
38. Wolverton, C. and Zunger, A., Comput. Mater. Sci. 8 (1997) 107.
39. Wolverton, C., Ozolins, V. and Zunger, A., Phys. Rev. B 57 (1998) 4332.
40. Alatalo, M., Weinert, M. and Watson, R. E., Phys. Rev. B 57 (1998) R2009.
41. Krause, J. C., Padvani, C., Schaff, J. and da Costa, M. I. , Phys. Rev. B 57 (1998) 587.
42. Ozolins, V., Wolverton, C. and Zunger, A., Phys. Rev. B 57 (1998) 6427.
43. Mayer, J., Meyer, B., Oehrens, J. S., Bester, G., Barnsen, N. and Fahnle, M., Intermetallics 5 (1997) 597.
44. Haas, H., Wang, C. Z., Fahnle, M., Elsasser, C. and Ho, K. M., Phys. Rev. B 57 (1998) 1461.
45. Farkas, D., Zhou, S. J., Vailhe, C., Mutasa, B. and Panova, J., J. Mater. Res. 12 (1997) 93, and references therein.
46. Mishin, Y. and Farkas, D., Philos. Mag. A 75 (1997) 169.

47. Gu, Q., Wang, Y. X., Wang, B. Y., Xu, G. Y. and Wang, T. M., Science in China Series E - Technological Sciences 39 (1996) 551.
48. Zhang, W. Q., Xie, Q., Ge, X. J. and Chen, N. X., J. Appl. Phys. 82 (1997) 578.
49. Moriarty, J. A. and Widom, M., Phys. Rev. B 56 (1997) 7905.
50. Besson, R. and Morillo, J., Phys. Rev. B 55 (1997) 193.
51. Sumin, V. V., Povarova, K. B., Fadeeva, N. V., Kazanskaya, N. K. and Bepaldova, M. D., Russian Metallurgy 1 (1997) 1998.
52. Mekhrasov, A. O., Akdeniz, M. V. and Arer, M. M., Acta Mater. 45 (1997) 1077.
53. Noebe, R. D., Bowman, R. R. and Nathal, M. V., Int. Mater. Rev. 38 (1993)193.

## Appendix A - BFS Parameterization

An advantage of the BFS method is that, due to its simple formulation, it allows for a straightforward (analytical) determination of the BFS  $\Delta_{AB}$  and  $\Delta_{BA}$  interaction parameters, therefore avoiding numerical uncertainties inherent to any numerical fitting procedure. Moreover, the input data used, whether it is obtained experimentally or from other theoretical calculations, ‘localizes’ the accuracy of the ensuing BFS predictions for those alloys in the vicinity of the phase diagram of the ordered structure used as input.

For simplicity, we reduce the following derivation to the case where the ordered structure corresponds to a cubic lattice characterized by a single lattice parameter  $a_0$  (simple bcc or fcc alloys with no tetragonal distortion).

Consider an alloy A-B, where due to the symmetry of the structure, there are  $N_X$  non-equivalent atoms of species  $X$  ( $X = A, B$ ) and  $n_{X_i}$  denotes the multiplicity of the  $i$ th non-equivalent atom of species  $X$ , so that

$$\sum_X \sum_{i=1}^{N_X} n_{X_i} = N_C \quad (A1)$$

where  $N_C$  is the total number of atoms in the cell. In this context, two atoms are deemed to be equivalent if they have the same environment within a sphere of radius  $R$ , the nearest-neighbor distance in the ground state crystal. In this case, the two conditions used to determine the BFS parameters consist of exactly reproducing the heat of formation  $\Delta H_0$  of the ordered structure and the corresponding lattice parameter, which are determined via LMTO calculations for a given structure [27,28]. In this work, we used the B2 NiAl base alloy as the basis for the LMTO calculation.



The two conditions are

$$\sum_X \sum_{i=1}^{N_X} \frac{n_{X_i}}{N_C} e_{X_i} = \Delta H_0 \quad (\text{A2})$$

and

$$\sum_X \sum_{i=1}^{N_X} \frac{n_{X_i}}{N_C} \frac{\partial e_{X_i}}{\partial a} \bigg|_{a_0} = 0 \quad (\text{A3})$$

where  $e_{X_i}$  represents the BFS contribution to the energy of formation, given by

$$e_{X_i} = e_{X_i}^S + g_{X_i}(e_{X_i}^C - e_{X_i}^{C_0}) \quad (\text{A4})$$

In Eq. A4,  $e_{X_i}^S$  is the BFS strain energy and  $\epsilon_{X_i}^C = e_{X_i}^C - e_{X_i}^{C_0}$  is the BFS chemical energy, where  $e_{X_i}^{C_0}$  is the reference energy.

For bulk ordered alloys, such as B2 NiAl, the BFS strain energy is the same for all atoms of the same species and it is uniquely determined by the input value of the lattice parameter  $a_0$ ,

$$e_{X_i}^S = E_C^X \left\{ 1 - (1 + a_{X_i}^{S*}) g_{X_i} \right\} \quad (\text{A5})$$

where

$$a_{X_i}^{S*} = \beta_X (a_0 - a_e^X) \quad (\text{A6})$$

where  $E_C^X$  and  $a_e^X$  are the cohesive energy and equilibrium lattice parameter, respectively, for atoms of species  $X$  and  $\beta_X = \frac{q}{l_X}$ , where  $q$  is a structure constant ( $q^3 = \frac{3}{8\pi}$  for bcc elements) and  $l_X$  is a scaling length for species  $X$  [24,25]. The coupling function included in Eq. A4 is given by

$$g_{X_i} = e^{-a_{X_i}^{S*}} \quad (\text{A7})$$

The BFS energy depends on the lattice parameter of the alloy structure only via the BFS strain energy and glue, therefore, Eqs. A2-A3 can be written as

$$\sum_X \sum_{i=1}^{N_X} \frac{n_{X_i}}{N_c} \left\{ e_{X_i}^S(a_0) + g_{X_i}(a_0) \epsilon_{X_i}^C \right\} = \Delta H_0 \quad (\text{A8})$$

and

$$\sum_X \sum_{i=1}^{N_X} \frac{n_{X_i}}{N_c} \left\{ \left. \frac{de_{X_i}^S}{da} \right|_{a_0} + \epsilon_{X_i}^C \left. \frac{dg_{X_i}}{da} \right|_{a_0} \right\} = 0. \quad (\text{A9})$$

Eq. A8 and A9 can then be written as

$$\sum_X \sum_{i=1}^{N_X} \frac{n_{X_i}}{N_c} g_{X_i}(a_0) \epsilon_{X_i}^C = \Delta H_0 - \sum_X \sum_{i=1}^{N_X} \frac{n_{X_i}}{N_c} e_{X_i}^S(a_0) \quad (\text{A10})$$

and

$$\sum_X \sum_{i=1}^{N_X} \frac{n_{X_i}}{N_c} \beta_X g_{X_i}(a_0) \epsilon_{X_i}^C = \sum_X \sum_{i=1}^{N_X} \frac{n_{X_i}}{N_c} E_C^X \beta_X a_{X_i}^{S*}(a_0) g_{X_i}(a_0) \quad (\text{A11})$$

If we concentrate now only on binary alloys that form fcc or bcc ordered structures characterized by a single lattice parameter ( $L1_2$ ,  $L1_0$ ,  $B2$ ,  $B32$ , etc.), then  $n_A + n_B = N_c$ . Simple expressions can then be obtained for the BFS chemical energies  $\epsilon_A^C$  and  $\epsilon_B^C$ :

$$\epsilon_A^C = \frac{\beta_B \delta_1 - \delta_2}{n_A g_A^{(0)} (\beta_B - \beta_A)} \quad (\text{A12})$$

and

$$\epsilon_B^C = \frac{\delta_2 - \beta_A \delta_1}{n_B g_B^{(0)} (\beta_B - \beta_A)} \quad (\text{A13})$$

where

$$\delta_1 = (n_A + n_B) \Delta H_0 - (n_A e_A^S(a_0) + n_B e_B^S(a_0)) \quad (\text{A14})$$

and

$$\delta_2 = \sum_X n_X \beta_X E_C^X g_X^{(0)}(a_0) \quad (\text{A15})$$

with  $g_X^{(0)} = g_X(a_0)$ . The BFS chemical energies can then be determined with Eqs. A12 and A13, so

that we can then search for the set of parameters  $(\Delta_{AB}, \Delta_{BA})$  that simultaneously satisfy these conditions. This is done by starting with the use of the following expression for the BFS chemical energy in terms of the equivalent (chemical) lattice parameter

$$\epsilon_X^C = \gamma_X E_C^X \left\{ 1 - (1 + a_X^{C*}) e^{-a_X^{C*}} \right\} \quad (\text{A16})$$

where  $\gamma = 1$  if  $a_X^{C*} > 0$  and  $\gamma = -1$  otherwise. The scaled lattice parameter for the chemical energy  $a_X^{C*}$ , given by

$$a_X^{C*} = \beta_X (a_X^C - a_e^X) \quad (\text{A17})$$

is related to the BFS parameters  $(\Delta_{AB}, \Delta_{BA})$  by means of the BFS equation for the chemical energy

$$NR_1^{p_X} e^{-\alpha_X R_1} + MR_2^{p_X} e^{-\left(\alpha_X + \frac{1}{\lambda_X}\right) R_2} = \sum_k N_{Xk} r_{X_1}^{p_X} e^{-(\alpha_X + \Delta_{kX}) r_{X_1}} + \sum_k M_{Xk} r_{X_2}^{p_X} e^{-\left(\alpha_X + \Delta_{kX} + \frac{1}{\lambda_X}\right) r_{X_2}} \quad (\text{A18})$$

where  $N(M)$  is the number of nearest-neighbors (next-nearest-neighbors) in the equivalent crystal of species  $X$ ,  $R_1 = ca_X^C$ ,  $R_2 = a_X^C$ ,  $r_1 = ca_e^X$  and  $r_{X_2} = a_e^X$  ( $c = \frac{\sqrt{3}}{2}$  for bcc). If we define

$$Q_X = N \left\{ r_{X_1} + \frac{ca_X^{C*}}{\beta_X} \right\}^{p_X} e^{-\alpha_X \left\{ r_{X_1} + \frac{ca_X^{C*}}{\beta_X} \right\}} + M \left\{ a_e^X + \frac{a_X^{C*}}{\beta_X} \right\}^{p_X} e^{-\left(\alpha_X + \frac{1}{\lambda_X}\right) \left\{ r_{X_1} + \frac{ca_X^{C*}}{\beta_X} \right\}} \quad (\text{A19})$$

$$q_1^X = N_{XX} r_{X_1}^{p_X} e^{-\alpha_X r_{X_1}} \quad (\text{A20})$$

and

$$q_2^X = M_{XX} r_{X_2}^{p_X} e^{-\left(\alpha_X + \frac{1}{\lambda_X}\right) r_{X_2}} \quad (\text{A21})$$

and considering the typical magnitude of the exponent in Eq.A21, it is reasonable to make the approximation  $r_{X_2} \approx r_{X_1}$  only in that term, then the l.h.s. of the BFS equation (Eq. A18) reads

$$Q_X - q_1^X - q_2^X = N_{XY} r_{X_1}^{p_X} e^{-(\alpha_X + \Delta_{YX})r_{X_1}} + M_{XY} r_{X_2}^{p_X} e^{-\left(\alpha_X + \Delta_{YX} + \frac{1}{\lambda_X}\right)r_{X_2}} \quad (\text{A22})$$

Let

$$q_d^X = N_{XY} r_{X_1}^{p_X} e^{-\alpha_X r_{X_1}} + M_{XY} r_{X_2}^{p_X} e^{-\left(\alpha_X + \frac{1}{\lambda_X}\right)r_{X_2}} \quad (\text{A23})$$

so that

$$Q_X - q_1^X - q_2^X \cong q_d^X e^{-\Delta_{YX} r_{X_1}} \quad (\text{A24})$$

then the BFS parameter  $\Delta_{YX}$  is given by

$$\Delta_{YX} = -\frac{1}{r_{X_1}} \ln \left\{ \frac{Q_X - q_1^X - q_2^X}{q_d^X} \right\} \quad (\text{A25})$$

This result is exact if second-neighbor contributions are not taken into account, or if for any particular structure  $M_{XY} = 0$  for all  $X$  and  $Y$ , as is the case in this work. The B2 structure is such that any given atom has an atom of its own species as a next-nearest-neighbor, i.e.  $M_{XX} = 6$  and  $M_{YX} = 0$ . With the exception of the numerical solution of Eq. (A16), the procedure for the determination of  $\Delta_{YX}$  using Eq. (A25) is straightforward and simple. Moreover, it can be easily shown that in most cases a quadratic approximation to the Rydberg function  $(1+z)e^{-z}$  suffices to guarantee accuracy up to 10 % of the exact results, with the added advantage of a completely analytical determination of the BFS parameters  $\Delta_{AB}$  and  $\Delta_{BA}$ . The parameters used in this work were obtained by following the procedure described in this Appendix, including second neighbor interactions and a numerical solution of the the transcendental equations involved.

## APPENDIX 2

In this appendix, we list the catalogue of configurations used in this work for different atomic distributions in a 72-atom cell, shown in Fig. 11. The B2 NiAl alloy corresponds to the atomic distribution shown in Fig. 11.a, where Ni atoms are denoted by black disks (labeled 1, 2, 3, ...) and the Al atoms are denoted with open circles (labeled 13, 14, 15, ...). A configuration is defined by changing the occupancy of these sites by exchanging atomic positions, substituting atoms of one species by atoms of the other species, or by introducing vacancies. The following table lists most of the configurations used in this work (only those used to construct the energy spectrum shown in Figs. 12 and 13). For example, a Ni atom in site  $n$  substituting for an Al atom in site  $m$  is denoted with  $\text{Ni}_n \rightarrow \text{Al}_m$ ;  $\text{V}_n$  denotes a vacancy in site  $n$  and  $\text{Al}_n \leftrightarrow \text{Ni}_m$  denotes an exchange of Al and Ni atoms between sites  $n$  and  $m$ . The configurations are listed according to their Ni concentration. The table also includes the values of the energy of formation of the configuration as well as its equilibrium lattice parameter (obtained by minimizing the energy of the cell with respect to  $a$ ).

$x_{\text{Ni}}$	Configuration	$\Delta H$ (eV/atom)	a (Å)
50.00	1. B2 NiAl	-0.60310	2.8500
	2. Ni <sub>31</sub> <-> Al <sub>42</sub>	-0.50816	2.8588
	3. Ni <sub>30,32</sub> <-> Al <sub>41,43</sub>	-0.41377	2.8678
	4. Ni <sub>30,32</sub> <-> Al <sub>42,43</sub>	-0.41261	2.8679
	5. Ni <sub>30,31</sub> <-> Al <sub>42,43</sub>	-0.43544	2.8656
	6. Ni <sub>1-9</sub> <-> Al <sub>13-24</sub>	-0.07384	2.9006
	7. Ni <sub>1,3,5,7,9,11</sub> <-> Al <sub>13,15,17,19,21,23</sub>	-0.16910	2.8914
	8. Al <sub>65-68</sub> <-> Ni <sub>53-56</sub>	-0.31271	2.8773
	9. Ni <sub>30,31</sub> <-> Al <sub>18,42</sub>	-0.44184	2.8650
	10. Ni <sub>31</sub> <-> Al <sub>42</sub>	-0.50814	2.8588
	11. Ni <sub>30</sub> <-> Al <sub>46</sub>	-0.49795	2.8597
	12. Ni <sub>30,31,34,35,54,55,58,59</sub> <-> Al <sub>14,17,19,22,62,65,67,70</sub>	-0.11404	2.8964
	13. Ni <sub>30,31,34,35,54,55,58,49</sub> <-> Al <sub>13,15,21,23,61,63,69,71</sub>	-0.06528	2.9011
	14. Ni <sub>50,54,58</sub> -> Al + Al <sub>62,66,70</sub> ->Ni	-0.09057	2.9050
	15. Ni <sub>30</sub> ->Al + Ni <sub>2,5,7,10,50,53,55,58</sub> <-> Al <sub>13,14,17,18,37,38,41,42</sub>	-0.06414	2.9020
51.39	16. Al <sub>42</sub> -> Ni	-0.59223	2.8457
	17. Al <sub>42</sub> -> Ni + [12]	-0.12280	2.8902
	18. Al <sub>42</sub> -> Ni + [13]	-0.06828	2.8955
	19. Al <sub>18,30,42</sub> -> Ni	-0.50607	2.8537
52.78	20. Al <sub>42,43</sub> -> Ni	-0.57990	2.8418
	21. Al <sub>42,44</sub> -> Ni	-0.58163	2.8416
54.17	22. Al <sub>38,42,46</sub> -> Ni	-0.56609	2.8380
	23. Al <sub>42-44</sub> -> Ni	-0.56781	2.8378
	24. Al <sub>42,46,47</sub> -> Ni	-0.56759	2.8379
	25. Al <sub>38,41,46</sub> -> Ni	-0.53671	2.8259

$x_{Ni}$	Configuration	$\Delta H$ (eV/atom)	a (Å)
55.55	26. Al <sub>38,40,61,63</sub> -> Ni	-0.56044	2.8335
	27. Al <sub>65-68</sub> -> Ni + Al <sub>61-64</sub> <-> Ni <sub>53-56</sub>	-0.33123	2.8541
	28. Al <sub>18,19,42,43</sub> -> Ni	-0.55365	2.8342
	29. Al <sub>38,39,41,42</sub> -> Ni	-0.55547	2.8340
	30. Al <sub>19,23,42,46</sub> ->	-0.55702	2.8338
	31. Al <sub>18,22,23,46</sub> -> Ni	-0.55523	2.8340
	32. Al <sub>65-68</sub> -> Ni	-0.55418	2.8341
Al-rich Ni <sub>(50-x)</sub> Al <sub>(50+x)</sub>			
$x_{Ni}$	Configuration	$\Delta H$ (eV/atom)	a (Å)
49.29	33. Ni <sub>31</sub> -> V	-0.43876	2.8426
	34. Ni <sub>31</sub> -> Al + Al <sub>42</sub> -> V	-0.45149	2.8474
	35. Ni <sub>31</sub> -> Al + Al <sub>46</sub> -> V	-0.42323	2.8518
48.57	36. Ni <sub>30,32</sub> -> V	-0.27055	2.8338
	37. Ni <sub>30,31</sub> -> V	-0.35110	2.8349
	38. Ni <sub>30</sub> -> Al + Ni <sub>31</sub> -> V + Al <sub>42</sub> -> V	-0.35407	2.8383
	39. Ni <sub>30,31</sub> -> Al + Al <sub>18,42</sub> -> V	-0.34075	2.8442
47.83	40. Ni <sub>26,30,34</sub> -> V	-0.34334	2.8276
	41. Ni <sub>30,31,32</sub> -> V	-0.26174	2.8263
	42. Ni <sub>30,34,35</sub> -> V	-0.24887	2.8281
47.06	43. Ni <sub>30,31,54,55</sub> -> V	-0.18313	2.8218
	44. Ni <sub>26,27,29,30</sub> -> V	-0.14426	2.8205
	45. Al <sub>65-68</sub> -> V + Ni <sub>53-56</sub> -> Al	-0.10201	2.8430
46.27	46. Ni <sub>5,29,30,31,32,53</sub> -> V	-0.09769	2.8070
	47. Ni <sub>5,7,29,31,53,55</sub> -> V	-0.06919	2.7960

REPORT DOCUMENTATION PAGE			Form Approved OMB No. 0704-0188	
Public reporting burden for this collection of information is estimated to average 1 hour per response, including the time for reviewing instructions, searching existing data sources, gathering and maintaining the data needed, and completing and reviewing the collection of information. Send comments regarding this burden estimate or any other aspect of this collection of information, including suggestions for reducing this burden, to Washington Headquarters Services, Directorate for Information Operations and Reports, 1215 Jefferson Davis Highway, Suite 1204, Arlington, VA 22202-4302, and to the Office of Management and Budget, Paperwork Reduction Project (0704-0188), Washington, DC 20503.				
1. AGENCY USE ONLY (Leave blank)		2. REPORT DATE November 1998		3. REPORT TYPE AND DATES COVERED Technical Memorandum
4. TITLE AND SUBTITLE  An Introduction to the BFS Method and Its Use to Model Binary NiAl Alloys			5. FUNDING NUMBERS  WU-523-22-13-00	
6. AUTHOR(S)  Guillermo Bozzolo, Ronald D. Noebe, J. Ferrante, and C. Amador				
7. PERFORMING ORGANIZATION NAME(S) AND ADDRESS(ES)  National Aeronautics and Space Administration Lewis Research Center Cleveland, Ohio 44135-3191			8. PERFORMING ORGANIZATION REPORT NUMBER  E-11426	
9. SPONSORING/MONITORING AGENCY NAME(S) AND ADDRESS(ES)  National Aeronautics and Space Administration Washington, DC 20546-0001			10. SPONSORING/MONITORING AGENCY REPORT NUMBER  NASA TM-1998-208820	
11. SUPPLEMENTARY NOTES  Guillermo Bozzolo, Ohio Aersospace Institute, 22800 Cedar Point Road, Cleveland, Ohio 44142; Ronald D. Noebe NASA Lewis Research Center; J. Ferrante, Cleveland State University, Cleveland, Ohio 44115; C. Amador Universidad Nacional Autónoma de México, Mexico D.F., Mexico. Responsible person, Ronald D. Noebe, organization code 5120, (216) 433-2093.				
12a. DISTRIBUTION/AVAILABILITY STATEMENT  Unclassified - Unlimited Subject Category: 26  This publication is available from the NASA Center for AeroSpace Information, (301) 621-0390.			12b. DISTRIBUTION CODE	
13. ABSTRACT (Maximum 200 words)  We introduce the Bozzolo-Ferrante-Smith (BFS) method for alloys as a computationally efficient tool for aiding in the process of alloy design. An intuitive description of the BFS method is provided, followed by a formal discussion of its implementation. The method is applied to the study of the defect structure of NiAl binary alloys. The groundwork is laid for a detailed progression to higher order NiAl-based alloys linking theoretical calculations and computer simulations based on the BFS method and experimental work validating each step of the alloy design process.				
14. SUBJECT TERMS  Intermetallics; Atomistic simulations; BFS method; Alloys			15. NUMBER OF PAGES 65	
			16. PRICE CODE A04	
17. SECURITY CLASSIFICATION OF REPORT Unclassified	18. SECURITY CLASSIFICATION OF THIS PAGE Unclassified	19. SECURITY CLASSIFICATION OF ABSTRACT Unclassified	20. LIMITATION OF ABSTRACT	